Synthesis of Two-dimensional Metal-Organic Frameworks and their Alloys

by

Shiljashree Vijay

A Thesis Presented in Partial Fulfillment
of the Requirements for the Degree
Master of Science

Approved April 2020 by the
Graduate Supervisory Committee:

Sefaattin Tongay, Chair
Matthew D. Green
Houlong Zhuang

ARIZONA STATE UNIVERSITY

May 2020

ABSTRACT

Metal-organic frameworks have made a feature in the cutting-edge technology with a wide variety of applications because they are the new material candidate as adsorbent or membrane with high surface area, various pore sizes, and highly tunable framework functionality properties. The emergence of two-dimensional (2D) metal-organic frameworks has surged an outburst of intense research to understand the feasible synthesis and exciting material properties of these class of materials. Despite their potential, studies to date show that it is extremely challenging to synthesize and manufacture 2D MOF at large scales with ultimate control over crystallinity and thickness.

The field of research to date has produced various synthesis routes which can further be used to design 2D materials with a range of organic ligands and metal linkers. This thesis seeks to extend these design rules to demonstrate the competitive growth of two- dimensional (2D) metal-organic frameworks(MOF) and their alloys to predict which ligands and metals can be combined, study the intercalation of Bromine in these frameworks and their alloys which leads to the discovery of reduced band gap in the layered MOF alloy.

In this study it has been shown that the key factor in achieving layered 2D MOFs and it relies on the use of carefully engineered ligands to terminate the out-of-plane sites on metal clusters thereby eliminating strong interlayer hydrogen bond formation.

The major contribution of pyridine is to replace interlayer hydrogen bonding or other weak chemical bonds. Overall results establish an entirely new synthesis method for producing highly crystalline and scalable 2D MOFs and their alloys. Bromine intercalation merits future studies on band gap engineering in these layered materials.

ACKNOWLEDGMENTS

I would like to express immense and sincere gratitude to my Faculty Chair, Prof. Sefaattin Tongay. Dr. Sef has shown incredible patience, abundant enthusiasm, wisdom, and endless support in molding my research work in my Master's study. My humble and sincere thanks go to Dr. Yuxia Shen for all the training, advice, and resources she has supported me throughout my research. Their passionate commitment to research work has majorly motivated me to put my best effort into my research. Tongay Lab at Arizona State University is my hub of research and motivation throughout my Master's thesis.

I would also like to thank Prof. Mathew D. Green and Prof Houlong Zhuang for serving as my committee members and their valuable contributions to this thesis. I would take this opportunity to also appreciate and thank all my lab peers, for all their advises and motivation in my research. Tongay Lab has always made us work with intense desire to discover new materials. This has constantly inspired me every day to learn and work at the lab which will always be memorable for me.

Most importantly I want to thank my parents and family for their unconditional love and support throughout my life.

TABLE OF CONTENTS

Page

CHAPTER Page

LIST OF FIGURES

Figure Page

Figure Page

Figure Page

CHAPTER 1

INTRODUCTION

1.1 Metal-Organic Frameworks

Metal-organic frameworks (MOFs) are a class of porous materials which were first developed in the 1990s.[26] With the advent of metal-organic frameworks into the world, they were even referred to as porous coordination polymers. After the further clarification in the difference between MOFs and coordination-polymers,[26,27] MOFs is the most accepted term from then onward. MOFs are hybrid materials consisting of metal clusters and organic ligands connected by coordination bonds. After the publishing the successful synthesis of MOF-5[28] and HKUST-1[29](Figure 1-1), MOFs were gaining peak attention. There was an explosion of research on MOFs towards their fascinating applications. MOFs are formed by coordination bonds between organic ligands and metal atom nodes with periodic structural units. Due to their structural characteristics, MOFs could provide the inherent advantages of both homogeneous and heterogeneous catalysts. Analogously to molecular catalysts, nano-dimensional porous MOFs possess well-defined chemical structures and readily accessible active sites. Also, MOFs are highly crystalline solid materials, which are conveniently recyclable and robust under both chemical and physical attack.[30-32]

After the first outbreak of MOFs first came into the world, Yagi reported the synthesis of Zn(BDC) (H_2BDC: Terephthalic acid also referred as Benzene 1,4 dicarboxylic acid or 1,4 Benzene dicarboxylate), showing a surface area around 270 m2/g (Langmuir).[41] Right after this publication, his group reported another new framework of

Zn and BDC, MOF-5 (IRMOF-1), showing a surface area at 2900 m2/g (Langmuir).[40] In 2004, Yagi's group again reported the synthesis of MOF-177 constructed by Zn clusters and 1,3,5-tris(4-carboxyphenyl)benzene (H3BTB) exhibiting an ultrahigh surface area of 4500 m2/g.[42]Simultaneously another group, Ferey et al. synthesized MIL-101 by reacting H_2BDC with Cr(NO3)3·9H2O at 220 °C for 8 hours. The activated sample shows a surface area as high as 5900 m2/g.[43] The world record of highest MOF surface area was reported by Hupp, synthesizing NU-110 with a surface area of 7000 m2/g.[44] Their group also presented a computational demonstration showing that the theoretically highest MOF surface area can reach to 14600 m2/g, which is adds to the size of almost 3 football fields in one gram of sample.

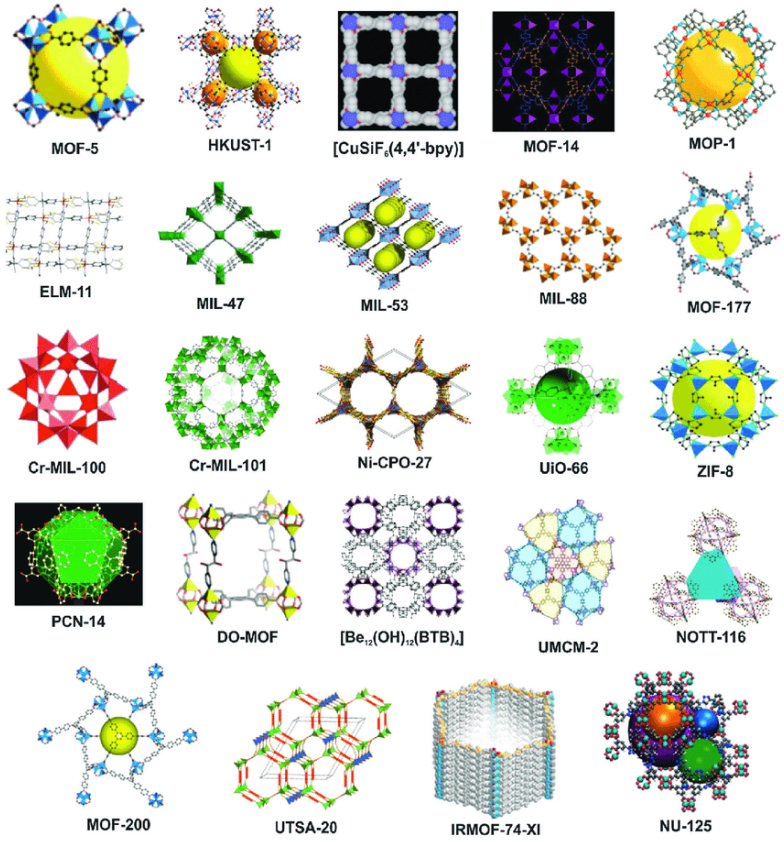

Figure 1-1 MOF Crystal structures.
Panel is adapted with permission from *Chem. Soc. Rev.*, 2015, 44, 6774--6803[109]

1.2 Applications of Metal-organic Frameworks

A shocking fact is that in the US, about 98 quads of energy is generated to power up human activities, and 10 – 15% of this energy is consumed by the chemical separation processes (Figure 1-2)[45]and 3% of the world energy consumption was devoted into distillation process.[46] As the energy consumption in the separation process is a mounting concern, we need to find a substitution for the conventional process that is more energy efficient. This is extremely meaningful and is in demand.

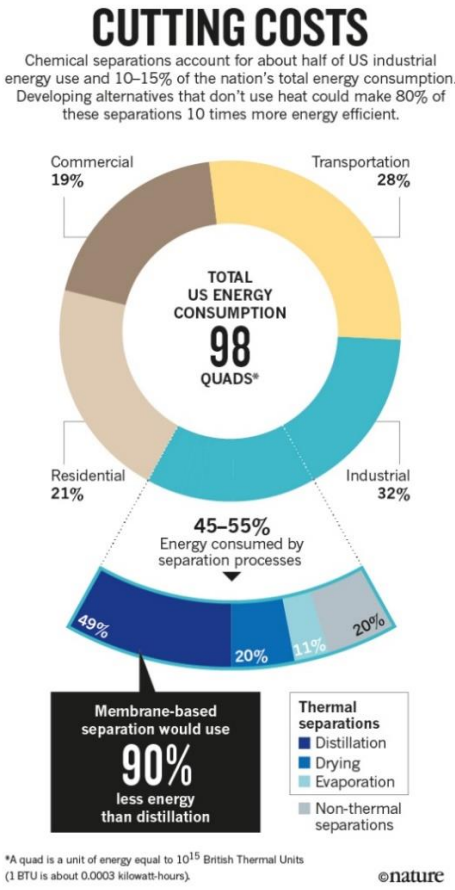

Figure 1-2 Energy consumption in US. Adapted by permission from Spring Nature: *Nature*, Seven chemical separations to change the world, David S. Sholl and Ryan P. Lively.[45]

MOFs can potentially outperform zeolites and carbons in many applications including gas storage, membrane separation, and adsorption separation. Energy gas storage is a very important topic for clean energy applications, including H_2 storage and CH_4 storage. It is reported by the DOE Office of Energy Efficiency and Renewable Energy in 2008 that, the US Department of Energy has a target set for the storage of hydrogen to be 0.055 kg H_2/kg system by 2020, which is ultimately 0.075 kg H_2/kg system (-40 to 60 °C).

In addition to the set target storage capacity, the adsorption and desorption process is required to be fully reversible for at least 1500 cycles with a fill time of 2.0 kg H_2/min system. The fundamental process known as physisorption is the key feature of MOFs that allows this fast and fully reversible adsorption/desorption process. Also, the storage capacity is highly dependent on the interacting surface area. The hydrogen storage process with the reliable preparation procedures, of MOF-5 is reported to be 7.1 wt% (by sample weight), with 1.67 kg/min loading speed.[47] Another report by Yagi's group says MOF-177 shows a H2 excess adsorption capacity of 7.5 wt% at 77 K and 70 bar.[48] NU-100 is the MOF with the highest surface area that has been tested for hydrogen storage .[49] Its hydrogen capacity is 9.95 wt% at 77 K and 56 bar.[50]The reported MOF H2 storage capacities versus surface area data is summarized in Figure 1-3[51]

MOF is a boon to the membrane separation technology. In addition to the chemical diversity and high surface area of the reported MOFs, the diversity of MOFs leads to another significant application to function as membrane separation materials. For porous materials-based membrane separation process, the separation is highly dependent on the adsorption-diffusion mechanism.[52]

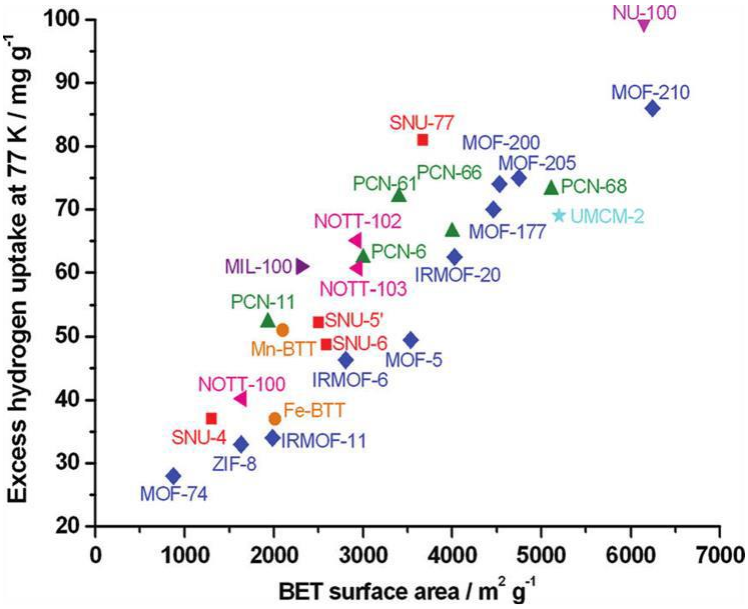

Figure 1-3 A citation report from Suh, Park, Prasad, & Lim, 2012, showing high pressure H_2 uptake capacities at 77 K versus BET surface.[103]

Besides the framework activity, the other important perception is that the porous crystalline structure serves as the molecular sieve with the pore size matching up with target molecules. The adopted porous material needs to have a pore size that precisely limits the access of at least one of the molecules to achieve a reasonable selectivity. It is reported that about 150 different types of zeolites, with a few number of zeolites being actually examined for practical applications.[53] Zeolites are different from MOFs wherein, MOFs that is made up of metal clusters and organic ligands, have theoretically countless blends, which extends to a large range of pore size corresponding to different separation targets.

Apart from the direct synthesis, post-synthetic modifications are also a feasible method to change their chemical properties and pore structures. By modifying the ligand's functional groups, detailed control over its pore size is attained. Though since the twentieth century MOF studies were established but to accomplish the synthesis procedures of MOF membranes were successful only until late twenty-first century. Keskin and Sholl in 2007 reported the first computational examination the application of MOFs in membrane separation.[54]Later in 2008, the first continuous MOF-5 membrane that can be used in gas separation was fabricated.[55]In the study report, the permeation of H_2, N_2, CH_4, CO_2, and SF6 were tested. MOF-5 showed a Knudsen diffusion behavior due to large pore size (around 1.56 nm).The zeolitic imidazolate framework (ZIF-95) membrane was fabricated by Caro's group(Huang et al., 2012) which had a 0.37 nm aperture, the fabricated membrane showed H_2 separation behavior much higher than Knudsen diffusion.[56] However, in comparison to the total number of MOFs reported, the number of studies on MOF based membranes are in a slow progress. Figure 1-4 depicts the distribution of publications on MOFs and their application in gas adsorptive separation from 1998 to 2017.[103] Similarly, when we search Web of Science, it shows the number of researches on metal organic frameworks to be more than forty four thousand, while using metal-organic frameworks membrane as keyword, the number of studies are just above two thousand. Currently, many MOF-based membrane studies are struggling through trial and error runs. It is still hard to fabricate a defect free MOF membrane and there is inadequate supporting information for the creation of high-quality MOF membranes. Only a limited number of structures have been successfully converted into membrane.

The field of research on high quality, defect free MOF membranes needs thorough investigation into the basic science of MOF synthesis to enhance the development of MOF-based membranes.

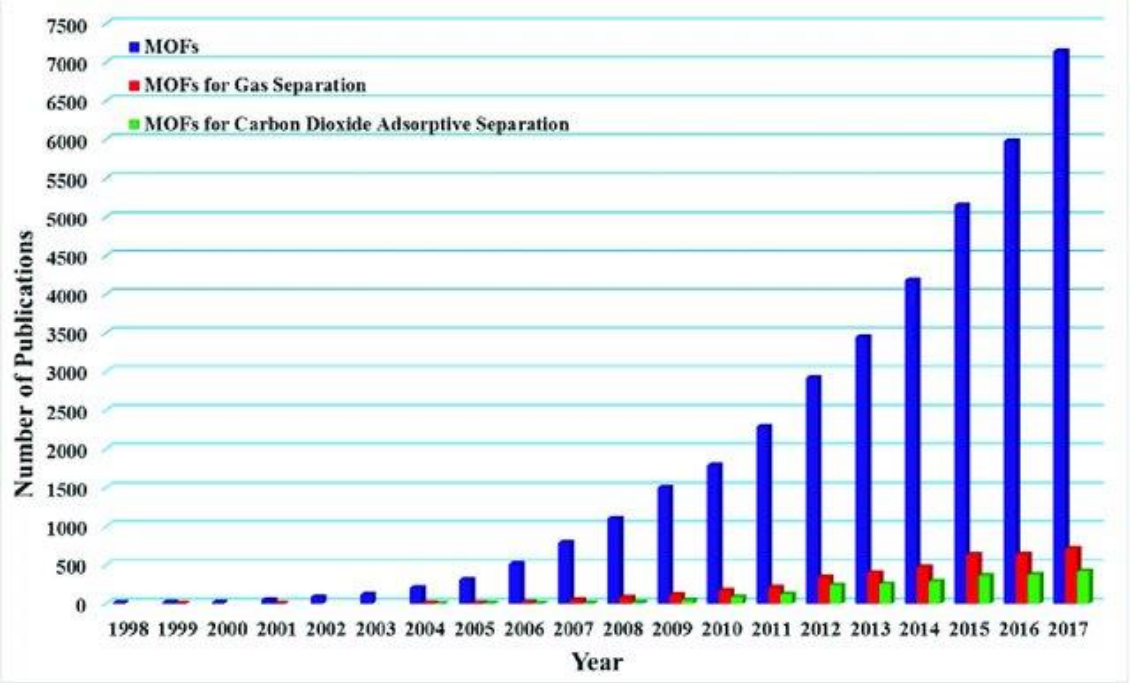

Figure 1-4 Distribution of publications on MOFs and their application in gas adsorptive separation from 1998 to 2017. Adapted with permission from Yilian Zheng et al 2018 IOP Conf. Ser.: Earth Environ. *Sci*. 170 032073[9]

As mentioned earlier, the high surface area materials that have good affinity towards target molecules are considered potential adsorbents. MOFs are the materials that have unprecedented high surface area as well as infinite possibility to produce high quality adsorbents. In recent years, with continued global warming and urgent need to reduce CO_2 emissions[57], a dedicated research effort has been devoted into CO_2 capture and separation by MOFs due to their highly tunable framework activity[58-63]and high energy efficiency compared to conventional separation methods, for example CO_2 removal from coal fired power plant emission and natural gas are among the top priorities[104].

There were many studies on post-synthetic modifications including ligand functionalization,[64,65] introducing open metal sites into framework,[67] and synthesis with strong CO_2 affinity ligands[66] that enhanced the CO_2 affinity to the framework. Chen's group reported synthesis and adsorption study of amine functionalized MIL-101(Cr) with an improved heat of adsorption of CO_2. Deng et al. have demonstrated Mg-MOF-74 with open metal sites can improve the CO_2/CH_4 selectivity.[67]After that, Feng's group endorsed the main-group metal-based MOF by reporting CPM-200-V/Mg with a CO_2/N_2 selectivity as high as 406.[68] Zhu et al. synthesized charged framework JUC-132, showing a high CO_2/CH_4 selectivity of 29.2 at 1 bar.[69] Another example of CO_2 capture via N-rich framework is mmen-CuBTTri reported by Long and other coworkers showing a CO_2 zero coverage heat of adsorption as high as -96 kJ/mol.[70] Rosi synthesized bio-MOF-11 using biomolecules, exhibiting a super high CO_2/N_2 selectivity of 75.[66]

Metal types with a wide variety have offered versatile functions in Metal-organic frameworks (MOFs). All the above-mentioned examples of discoveries of MOFs have paved way for an emergent scientific field to explore their potential applications and inspired the researchers into producing various types of frameworks with different combinations of metal types to explore their exciting properties.

1.3 Introduction to the world of 2D polymers

The discovery of graphene led to a new field of research in organic/inorganic chemistry and materials science dedicated to synthesizing and characterizing two-dimensional (2D) materials material systems of either inorganic or organic families have garnered tremendous research interest.[1]

Inorganic 2D materials such as transition-metal dichalcogenides (TMDs),[2] hexagonal boron nitrides (h-BN),[3] MXenes,[4–8] and layered perovskites[9] have demonstrated exotic quantum properties for applications in optoelectronics, energy harvesting materials, flexible electronics, spintronics, luminescence devices, and sensors. However, these materials lack flexibility in their structural, chemical design and porous behavior when compared to their polymeric counterparts[10]. A 2D polymer is usually defined as a topologically planar molecular sheet constructed by linked, repeating units of building blocks/ monomers that extend across two dimensions. Sometimes, the 2D definition also includes a few layers of stacked 2D sheets interacting through weak van der Waals (vdW) forces.[11] From a physical perspective, their ultrathin nature often means that quantum electron confinement effects are much more prominent, which gives rise to many novel optical, electronic, thermal, and magnetic phenomena.[12] Extensive research is being done on synthetic 2D polymers for their unique material properties and rational synthesis methods.

1.4 Overview on 2D materials and 2D MOFs

Although after the discovery of many 2D materials, graphene remains one of the world's most popular in demand and intriguing material. Graphene is a crystalline 2D allotrope of carbon atoms with sp^2 hybridization and it forms a hexagonal lattice. Like most layered materials, graphene can be synthesized by simple methods like liquid or mechanical exfoliation, and by challenging methods, such as chemical vapor deposition (CVD).[13]

Compared to the form of bulk graphite, graphene has many necessary physical and electronic properties that can explore pathways to a wide variety of applications. A single sheet of graphene possesses astonishing mechanical properties due to the stability of the sp^2 bonds which greatly opposes a variety of in-plane deformations. A defect-free monolayer membrane measured an intrinsic strength of 42 Nm^{-1} and a Young's Modulus of 1 TPa, which is many times stronger and lighter than steel.[14] The incorporation of graphene particles into nanocomposites has demonstrated significant enhancement to their mechanical properties due to its high aspect ratio and intrinsic mechanical strength.[15]

Along with its excellent mechanical properties, graphene is a zero-band gap semiconductor with high intrinsic electron mobility, electronic conductivity, optical transmittance, and thermal conductivity. These unique properties can allow for the potential advancement of transparent electronics, field-effect transistors, energy storage, bio-sensors, and water filtration technologies.[16–20] Although there are many possible applications with graphene, its lack of a band gap severely limits its use in electronic switch control since a band gap allows for control and manipulation of electron flow in electronics. There have been recent developments in strain engineering, chemical functionalization, and manipulation of graphene architectures to widen the band gap.[21–23] Even with these efforts, the lack of a wider band gap has directed researchers into investigating other 2D materials with semiconducting character.

Under the 2D polymer umbrella, 2D coordination polymers (CPs) are one of the subclasses of organic materials that are constructed by tiling organic ligands with metal ions in the two-dimensional landscape.

In the research literature, these 2D CPs are also commonly referred to as 2D metal-organic frameworks (2D MOFs), coordination nanosheets (CONASHs), and even metal-organic layers (MOLs). Both 2D CPs and covalently bonded organic polymers can be selectively synthesized with defined and tunable chemical functionalities to have a variety of diverse material properties. 2D CP networks are essentially the product of Lewis acid-base pairs in which the organic ligands are bonded to a central metal ion through coordinate covalent bonds. In comparison to strictly covalently bonded 2D polymers, the insertion of a metal linker into the organic framework allows for p-d orbital interactions to contain unique electronic, magnetic, and optical properties. The weak and reversible interactions of coordination bonds of 2D CPs also allow for the self-assembly of the organic ligands and metal linkers.[10,11,24,25]

2D Transition metal dichalcogenides (TMDCs) are promising alternatives to graphene 2D material. They have a stoichiometric formula, MX_2, where M is a transition metal atom from group IV (Ti, Zr, or Hf), group V (V, Nb, or Ta) or group Vi (Mo or W) and X is a chalcogen (S, Se, or Te). TMDCs are layered materials that can be mechanically exfoliated to single sheets due to the weak interlayer van Der Waals interactions or it can be synthesized from chemical vapor deposition. In monolayer form, many of these 2D TMDCs exhibit a direct bandgap, strong spin-orbit coupling, and favorable electronic and mechanical properties.[33] Depending on the elemental compositions, these materials can exhibit semiconducting (MoS_2, WS_2, etc.) or metallic behavior (VSe2, NbS2, etc.).[33] Due

to the quantum confinement effect, the band structure of these 2D materials can be tuned as the number of layers shrinks down which brings down to the typical electronic structures of these materials.

For example, the MoX_2 and WX_2 class TMDCs exhibit a widening of the band gap with decreasing atomic thickness and, ultimately, a transition from an indirect band gap to a direct band gap is in the monolayer limit.

MoS_2 monolayers were grown in the lab using the CVD method based on Zande et al.'s set-up and sodium chloride (NaCl) assisted growth based on other literature.[34,35] Figure 1-1a shows the set-up for this particular synthesis. This process was optimized to produce the largest and cleanest MoS_2 monolayered triangles, optically shown in Figure 1-1b.

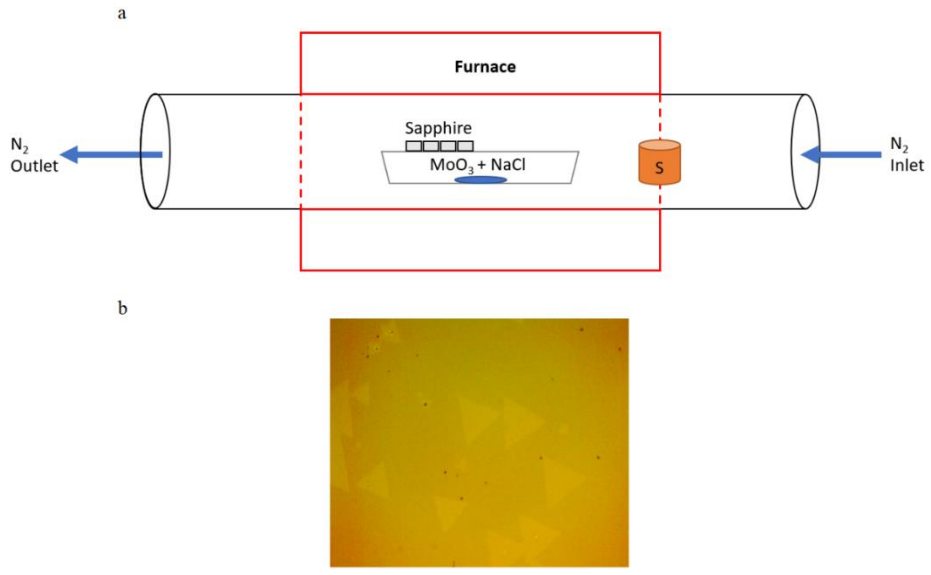

Figure 1-5 a) Schematic of set-up used in CVD of MoS_2 b) Optical image of MoS_2 crystals

A review on by far reported experimental methods of 2D coordination polymers will be introduced in Chapter 2. The main synthesis of monolayer and stacked layers of coordination polymers and their characterization techniques are discussed in Chapter 2.

Recently, atomically thin layered organic frameworks are rising as an attractive subcategory of two-dimensional (2D) materials. Like the conventional 2D materials, MOFs can behave as 2D crystals as well. As a new emerging research area, the number of investigations on 2D MOFs have increased dramatically in the past five years.

Besides the investigation of the basic performance of these materials to pave the way for their advanced applications, the most attractive point of using 2D MOFs are membrane separation and catalysts. For membrane separation, to reach a point where the permeability and selectivity compromise in a perfect way, people appreciate the thickness of the membrane is reduced to an extreme point that one single molecule thickness would be the best case. Like the mixed matrix membranes with 2D fillers, an increasing attention has been given to the 2D MOF based mixed matrix membrane. In 2014, the synthesis of 2D Copper 1,4-benzenedicarboxylate (CuBDC) was produced and the obtained 2D nanosheets were incorporated into the Matrimid polymer matrix. The fabricated mixed matrix membranes were used for CO_2/CH_4 separation.[36]

Recently, research scholars started to systematically investigate the synthesis methods of 2D MOFs. The synthesis methods are called as two types, 1) top-down method and 2) bottom-up method. The top-down method refers to the synthesis of bulk 2D crystals followed by a thinning down process to generate 2D MOF nanosheets.

The top-down method is easy to operate and can potentially produce large quantities of 2D nanosheets. However, the thinning down process requires a rigorous exfoliation, including sonication or chemical intercalation. As a result, the obtained sample is normally small and contains many defects. The fragmentation would produce a broad particle size distribution.

In 2011, Li et al. reported the top-down method to produce MOF-2 nanosheets. [37] While, the bottom-up method is the opposite process, which can generate the MOF nanosheets directly. The obtaining of the nanosheets is through the detailed control of its synthesis process. Currently, the popular processes are limiting the diffusion process or reaction area.

Dong and coworkers reported the Langmuir-Blodgett method to produce 2D Ni-based super-molecular polymer.[38]The single layer thick sample in micrometer level dimension was obtained at the air-liquid interface. Also, in 2015, the 2D Porphyrinic metal-organic frameworks (2D M-TCPP) where M = Zn, Cu, Cd, or Co was synthesized using the surfactant-assisted synthesis. It was proposed the addition of surfactant promotes the anisotropic growth. Since the modification of the synthesis method requires a design of reaction based on a comprehensive understanding of material properties, only a limited number of studies were reported by now, and yields are low in most of the cases.

The construction of MOFs with two different metal types (bimetallic MOFs) that maintain their overall crystalline structure is desirable because the adjustable alloy composition may, in turn, afford markedly improved properties.

A few advantageous examples include enhanced nitrogen sorption for bimetallic HKUST-1 with respect to its sole-metal counterparts[109] and improved Li-O_2 batteries performance in terms of their discharge/charge reversibility and efficiency which are contributed by bimetallic Mn/Co in MOF-74[24]. Notably, although the potential in applications of bimetallic MOFs is attractive, their synthesis is mainly empirical and limited to few metals.

The investigation of a fast and generic method to produce 2D MOFs has tremendous meaning for the field to advance the applications in various directions.[39] In Chapter 3, a detailed investigation of synthesis of 2D MOF crystals and their alloys will be given. We proposed a novel synthesis method that comprises the employment of pyridine, a capping agent to control the anisotropic growth MOFs that can be potentially used in a wide variety of MOFs.

Also exploring the synthesis by single phase and bi-phase methods allowed us to resolve the trade-off between crystallinity and yield. The obtained high quality 2D MOF nanosheets allowed us to carry out a more detailed study of their fundamental properties.

CHAPTER 2

REVIEW OF EXPERIMENTAL METHODS

2.1 Synthesis and manufacture of 2D MOFs

Preparation methods of 2D Coordination Polymers (CPs) have garnered a great deal of interest in the past decade. In this section, the main synthesis techniques used for both monolayer and stacked sheets of CPs (vdW CPs) will be introduced and discussed.

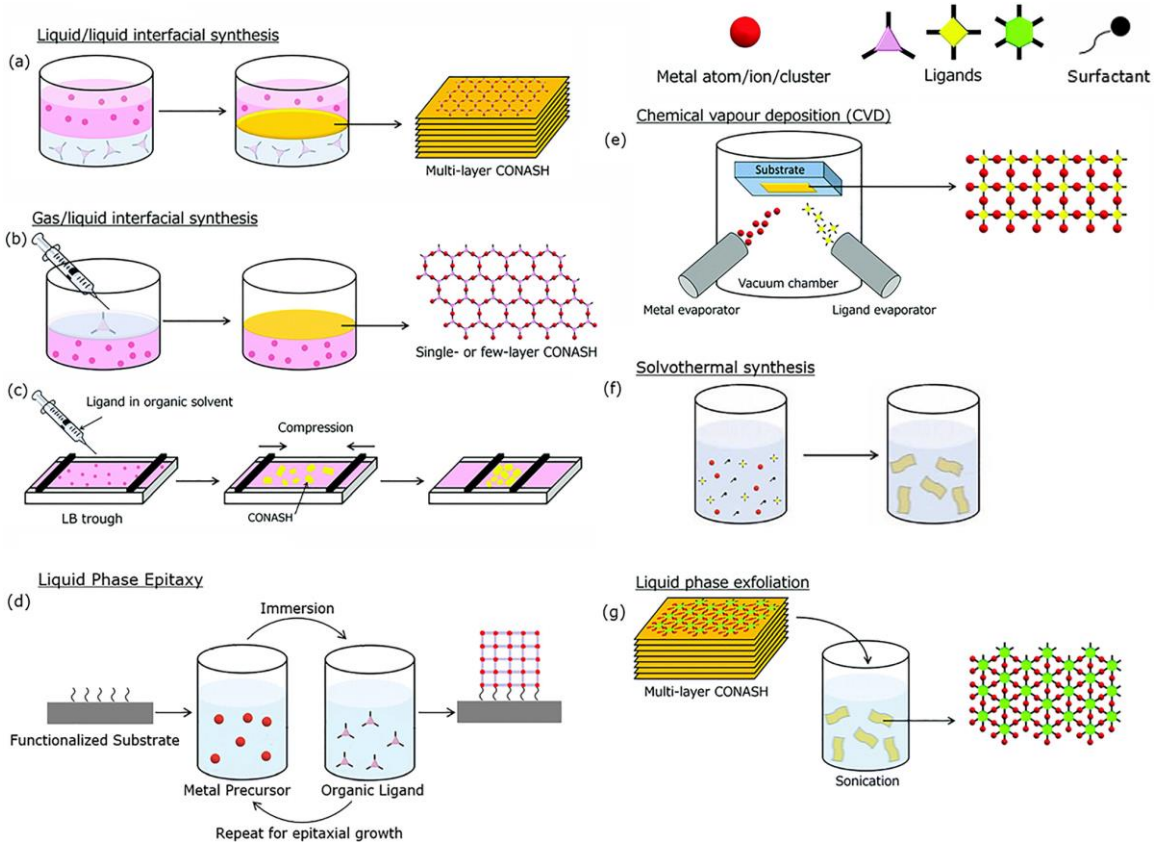

Figure 2-1 Schematic illustrations of (a) liquid/liquid interfacial synthesis, (b) and (c) gas/liquid interfacial synthesis (d) liquid phase epitaxy (solid/liquid interface), (e) CVD synthesis, (f) solvothermal synthesis, and (g) liquid-phase exfoliation. Adapted with permission from Sakamoto et al., *Chem. Commun*. 53, 5781 (2017). Copyright 2017 Royal Society of Chemistry.[10]

Articles, such as by Cao et al. and Zhao et al., that provide greater details on the methods as well as dozens of examples of the synthesized 2D CPs.[71-73] considering these existing review articles, the focus of this review will be given to those methods that have emerged over the years as the best in terms of manufacturability and compatibility with the industry which is summarized in Fig. 1.[10]

2.1 a Liquid/liquid interface

In a liquid-liquid interfacial synthesis, an aqueous solution of the metal salt is deposited on an organic solution containing the ligand. Then, the ligands and metal ions undergo coordination reactions at the interface of the two immiscible solutions, producing a suspended thin film [Figure 2-1(a)]. The film can be extracted onto a substrate or filtered out.

Chen et al. fabricated Ag and Au benzene-hexathiol (BHT) 2D CPs by a liquid-liquid interfacial reaction in an aqueous sodium hydroxide solution and a co-solvent mixture of acetonitrile and ethyl acetate.[74,111] Silicon/silicon dioxide substrates were placed into the solution and the film was deposited as the solvent and was aspirated. The synthesis produced 276 nm thick Au-BHT films and 324 nm thick Ag-BHT films with lateral sizes up to 100 micro-meters. This method can produce larger lateral films than the gas/liquid interfacial methods but tend to have an increased thickness due to diffusion and mixing at the interface.[10]

2.1 b Gas/liquid interface

In a typical gas/liquid interfacial synthesis, a thin layer of organic solution containing the ligand is spread onto an aqueous solution containing the metal salt. As the organic solvent is evaporated, the metal ion and organic ligand are confined to form coordination bonds at the interface, yielding the 2D CP [Figure. 1(b)]. [10]The 2Dfilmcan be picked up by a substrate in a lift-up method. The Langmuir-Blodgett film technique is also popular as it allows for the CP thickness and orientation to be controlled mechanically.[73] In this case, the CP sheet(s) can be prepared by slowly compressing the solvent to form the film [Fig.1(c)]. [10]The 2D CP is then transferred from the liquid-gas interface onto a solid substrate. Makiura and Konovalov demonstrated this process with the reaction between tetra-pyridyl-porphyrin zinc (Zn-TPyP) in a mixed chloroform-methanol solvent and Cu ions in water within a Langmuir trough.19 The carefully controlled surface pressure of the trough produced molecularly thin sheets with domain sizes of approximately 410 nm.[10] The gas/liquid interfacial synthesis has successfully formed many monolayer and stacked sheet CPs.[10,74-76,111]

2.1 c Solid/liquid interface

A more recent synthetic approach is liquid phase epitaxy, which involves the solid-liquid interface. Epitaxial growth of 2D CPs requires flat substrates functionalized by surfactant molecules.[10]The functionalized substrate becomes a template for fabricating self-assembled monolayers (SAMs). This method involves the use of surfactant molecules that can self-adhere as a monolayer onto a metal/metal-oxide substrate with the free functional groups serving as the nucleation sites for coordination polymer assembly.

An example includes functionalizing metal substrates with thiol molecules or hydroxyl molecules that will be used as a nucleation-directing template. Gu et al. offers an extensive review on various established epitaxial growth techniques of 2D CPs.[77,78] The most common and flexible method involves the dipping layer by layer method, wherein the SAM undergoes an alternating sequence of simple immersion processes into solutions containing either the metal ion or organic ligands.[79,80] The self-assembly of the CPs will occur layer by layer on the functionalized substrate with each immersion into the solution.

Recently, Wang and co-workers developed a layer-by-layer epitaxial growth protocol to synthesize 2D zinc tetracarboxylate-porphyrins (TCPP) for solar cell applications.[78] The group started with a fluorine-doped tin oxide substrate (FTO) functionalized with hydroxyl groups. Like the process shown in Fig. 1(d), the procedure involved cyclic immersions of the FTO substrate into a zinc acetate solution, then ethanol, then a porphyrin solution, and then ethanol again. The thickness was controlled from a single layer to 200 nm by controlling the number of immersion cycles. The FTO with thin film Zn-TCPP was then directly integrated into a dye sensitized solar cell. Epitaxial growth allows for increased orientation and thickness control, although the material properties will be affected by the substrate and chemical functionalization.[10]

2.1 d Top-down techniques

In contrast to bottom-up techniques, this method starts with bulk vdW crystalline materials containing 2D stacked layers held together by weak interlaminar forces. Individual monolayers are isolated by mechanical exfoliation or by a liquid delamination process. [10]

While micromechanical exfoliation is one of the most popular top-down approaches for 2D materials, generally liquid phase exfoliation (LPE) first comes to mind among top-down methods of 2D CPs.[10] LPE involves ultrasonication to delaminate larger 2D crystals/powders in solvent and produce a colloidal suspension of the sheets [Fig. 1(e)].[81-85] LPE can be further manipulated by crystal-solvent chemistry to control the exfoliation process. In general, the surface energies of the solvent and sheets should match to encourage exfoliation and stabilization of the suspended sheets. An example is the use of water or alcohol to delaminate 2D CPs held together by interlayer hydrogen bonds.[74,111]Recently, Mukhopadhyay and co-workers exfoliated layered CPs consisting of 2,2-diphenylbenzopyran ligand backbones with pyridyl/carboxylate functionalities and Cd/Zn linkers.[86] The bulk powders were first synthesized through solvothermal conditions, forming layered CPs with pores occupied by solvent molecules. Due to the hydrophilic nature of the carboxylate functionalities, LPE was performed in ethanolic solutions. The LPE proceeded for 30min and produced 3–6 nm thick sheets with lateral sizes around 500 nm.[10]

2.2 Sample Characterization Methodologies

After sample preparation and crystal growth formation, various characterization techniques were employed to identify the 2D MOF, its crystallinity, thickness, and morphology. Raman spectroscopy, X-ray diffraction, Atomic force microscopy X-ray photoelectron spectroscopy and Scanning tunneling microscopy were utilized to analyze the properties. In this section, a brief overview of each technique will be introduced.

2.2 a Raman Spectroscopy

Raman spectroscopy is a non-destructive analysis technique that provides the specific fingerprint to identify materials through the analysis of their vibrational modes. In addition, it can be used to analyze the crystallinity, orientation, presence of defects, thickness and strain of materials. The wealth of information this method provides makes it a staple characterization tool for 2D MOFs.

The principle behind Raman scattering and typical spectroscopic set-up is shown in Figure 2-2. When a sample is irradiated with a monochromatic source of light, there are light-matter interactions that will result in reflected, absorbed, or scattered light. Scattered light can be separated into elastic and inelastic scattering. Elastic scattering is the dominating process and occurs when the photons interact with the material and retain their original energy state. This is called Rayleigh scattering and is typically filtered out of the spectrometer. For inelastic scattering, a small portion of the scattered light interacts with the material and exchanges energy. This exchange of energy results in two different inelastic scattering mechanisms, Stokes and Anti-stokes scattering. Anti-stokes Raman scattering occurs when the molecular vibration of the molecule transfers to the photon; however, this process is energetically less likely to occur and generally not collected. In Stokes scattering, the incident photons lose a portion of their energy to lattice vibrations. The amount of energy transferred to excite the vibrational mode (phonons) is exact and this information is collected through a charged coupled detector to generate a plot showing peak intensity against wavenumber (cm^{-1}). The location, intensity, and their full width at half maximum (FWHM) can provide information on the identity, crystallinity, and relative quantity of the material.

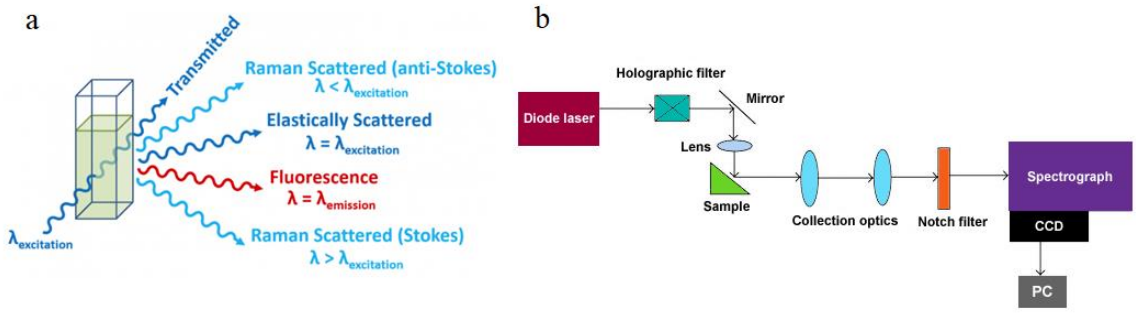

Figure 2-2 a) Schematic representation identifying the light scattering mechanisms after laser exposure to sample[89] b) Schematic of general Raman set-up[90]

2.2 b X-ray diffraction

X-ray diffraction (XRD) is a common method to identify the crystal structure and periodicity of 2D materials. A schematic representation on XRD principle is given below in Figure 2-3.

Powder X-ray diffraction (PXRD) is typically used for powder and thicker samples, providing lattice information on the layered structure. However, this method is not as useful in characterizing thin films and few-layer sheets. Grazing incidence X-ray diffraction (GIXRD) with synchrotron radiation is recommended to obtain diffraction of ultrathin materials. This method uses small incident angles for incoming X-rays to limit penetration and encourage diffraction at the surface.[10]

Huang and co-workers demonstrated GIXRD characterization on a 60 nm thin nanosheet to determine the interlayer distance and crystal lattice structure that matched theoretical predictions.[87]

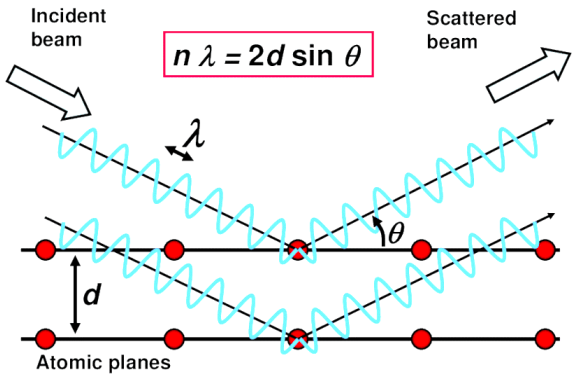

Figure 2-3 Schematic representation on XRD principle.

2.2 c Atomic Force Microscopy (AFM)

AFM is a main microscopy technique that can perform surface characterization of most flat materials at nanoscale resolution. This tool can be used for imaging of material topography, phase change, thickness, thermal and electrical conductivity, magnetism, and piezoelectric behavior. A typical AFM set-up is shown in Figure 2-3. In our AFM system, a piezoelectric scanner controls the cantilever and probe There is a reflective coating on the topside of the cantilever that reflects light, which is detected by a photodiode. As the tip moves across the sample, the cantilever moves vertically up and down due to the local forces between the tip and sample. The reflected light mirrors the cantilever motion, and the signal is recorded by the detector. The topography of the surface can be imaged by raster scanning of the sample and recording of the probe height while holding the signal of the probe-sample interaction constant. AFM can operate in contact, tapping, or non-contact mode. Generally, tapping and non-contact modes are preferable on softer materials but may produce lower lateral resolution images.

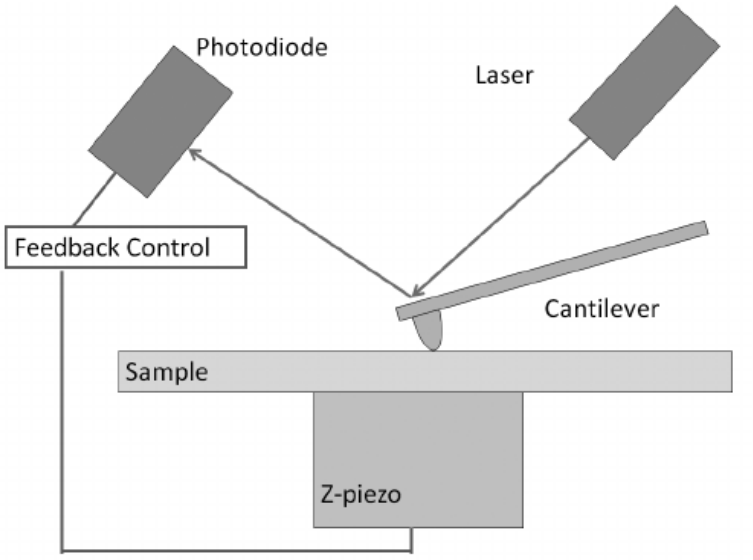

Figure 2-4 Typical AFM set-up[88]

2.2 d X-ray photoelectron spectroscopy

X-ray photoelectron spectroscopy (XPS) is a technique that probes the chemical composition and bonding environment. This method analyzes the energy of the photoemitted electron at the surface making it suitable for 2D CPs with nanoscale thicknesses. For example, XPS was utilized by Lahiri and co-workers to confirm the composition of a 2D nickel hexa-aminobenzene (HAB) CP.[91] The scan confirmed the presence of all the involved elements (C, N, and Ni) as well as the oxidation state of the Ni in the complex.[10]

2.2 e Scanning tunneling microscopy

Scanning tunneling microscopy (STM) is used to image surfaces at an atomic scale. This method can probe individual atoms based on the local density of states on the surface of the sample based on the principle of quantum tunneling.

Kumar and co-workers applied STM characterization to a 2D CP consisting of dicyanobiphenyl (DCBP)/ dicyanoanthracene (DCA) ligands with cobalt metal linkers grown on weakly interacting substrates such as graphene.[92]Their work showed clear images of the 2D CP's honeycomb periodicity (Fig. 2). From the STM images, the coordination bond lengths and lattice constants were extracted. The group combined additional scanning tunneling spectroscopy data with density functional theory (DFT) calculations to investigate the intrinsic electronic properties and band structure of the 2D CP.[10]

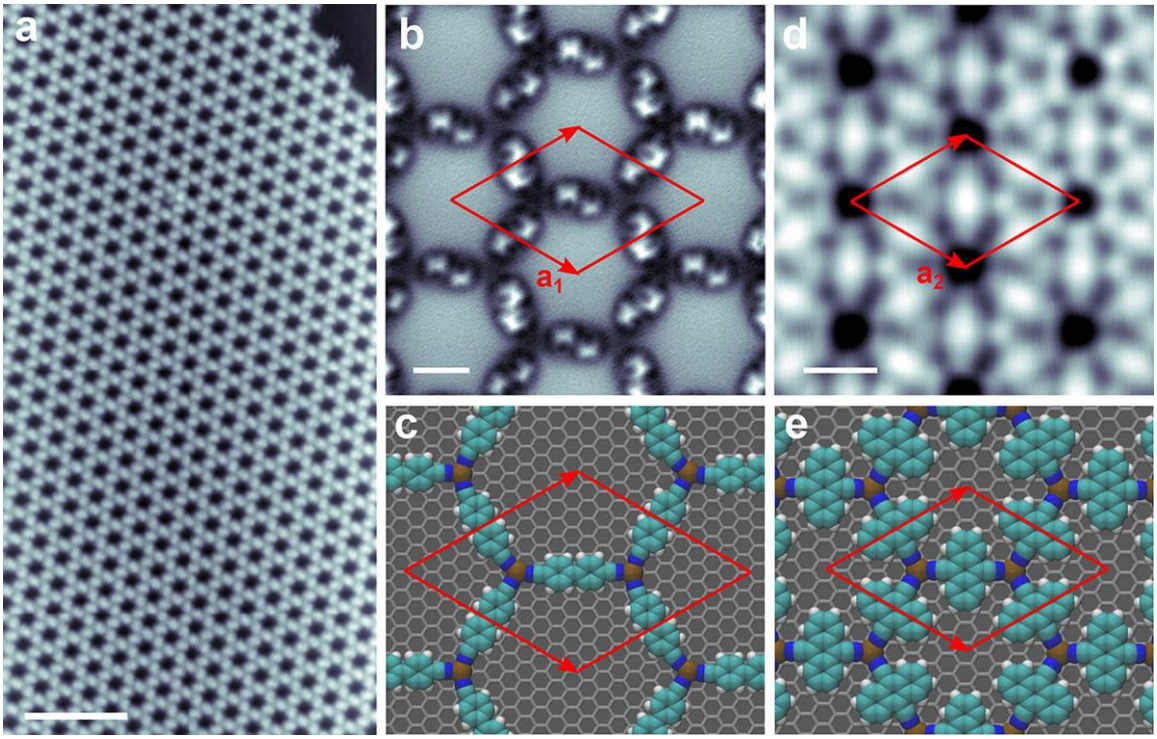

Figure 2-5 Overview of two MOFs. (a) An STM overview image of a honeycomb DCBP3Co2 MOF on a G/Ir(111) surface. The scale bar is 10 nm. Imaging parameters: 1.23 V and 3.3 pA. (b) Constant height frequency-shift, Df, nc-AFM image of DCBP3Co2 MOF acquired with a CO-terminated tip. The scale bar is 1 nm. (c) DFT-simulated structure of the DCBP3Co2 MOF on graphene. (d) STM topography image of the DCA3Co2 MOF. The scale bar is 1 nm. Imaging parameters: - 1 V, 15 pA. (e) DFT simulated structure of the DCA3Co2 MOF on graphene. Red parallelograms indicate the unit cells. Reproduced with permission from Kumar et al., *Nano Letters* 18, 5596–5602 (2018). Copyright 2018American Chemical Society.[92]

CHAPTER 3

SYNTHESIS OF TWO-DIMENSIONAL (2D) METAL-ORGANIC FRAMEWORKS AND THEIR ALLOYS

3.1 Introduction

2D Metal-organic frameworks (2D MOFs) offer advantages of both 2D layers and traditional MOFs and have received tremendous attention due to their organic–inorganic hybrid nature, large surface area, highly exposed active sites, and ultrathin thickness. [105] Metal-organic frameworks that are atomically thin layered are a sub-category of two-dimensional (2D) materials which can be constructed by coordination bond formation of monomers or by inorganic metal clusters and organic linkers to form 2D polymer and 2D metal-organic frameworks (2D MOFs), respectively.[101]

Metal types with a wide variety have offered versatile functions in Metal-organic frameworks (MOFs). The ability of MOFs to capture and store molecular species has led to their application in CO_2 sequestration, storage of hydrogen and in drug delivery. The presence of transition metal atoms possessing unfilled d-orbitals that generate open metal sites (also referred to as coordinatively unsaturated metals) play vital roles in specific recognition of small molecules is highly attractive from a catalysis and sustainability applications perspective.[93]. Also, high crystalline porous structure within the 2D plane has promising applications in gas sensing and membrane separation and selective gas separation applications. [94] Lastly, 2D MOFs can be isolated down to monolayers and owing to their mechanical flexibility, they can be implemented into a variety of optoelectronic applications.[95] Notably, although the potential in applications of bimetallic MOFs is attractive, their synthesis is mainly empirical and limited to few metals.

It is evident that 2D MOFs have a tremendous amount of applications, despite their amazing potential, research studies throughout mentions challenges in scaling up of synthesis and large-scale production of 2D MOFs with ultimate control over their crystallinity and thickness. Their 2D nature offers unique advantages over conventional 3D MOFs in that they have a large surface to volume ratio offering high surface reactivity/sensitivity. Controlling over interlayer binding energy is a solution to realize the construction of 2D MOFs at large scale.

The most interesting and innovation research work by Kitagawa's team demonstrated the liquid/air and liquid/liquid interfaces of 2D MOF crystal growth of NAFS-1 and NAFS-2 nanofilm.[96]Another interesting study by Gascon developed a three-phase strategy in which metal cation (Cu^{2+}) and organic ligand (carboxyl groups) were localized into two liquid layers and separated by a third layer.[97]Other complementary methods, such as ultrasonication[98] and chemical intercalation,[99] were utilized to yield ultra-thin MOFs, however these studies only lead to the production of small scale 2D MOFs. As such, many fundamental questions remain open for scalable manufacturing of 2D MOFs: i) How to attain control over the bonding nature (vdW, hydrogen, or chemical bonding) between layers to produce weakly coupled 2D nano-sheets? ii) How to optimize the synergistic effect among the metal clusters, ligands and other reaction additives to avoid the tradeoff between productivity and crystallinity without compromising on its aspect ratio? and iii)However, how to involve two different metal ions within the 2D landscape?

In this chapter, the governing effects of interplanar hydrogen bonds induced by coordinated water molecules on the framework dimension (i.e conversion from 2D to 3D) of MOF-2 are demonstrated. Replacing water with pyridine is a critical step to attain layered MOF-2D structures while adding a controlled amount of triethylamine (TEA) and formic acid which forms the basis tuning kinetic reaction constants by adjusting the proton concentration. These results and established synthesis route enable large scale strategy to realize the layer-by-layer growth of 2D MOF-2 with high yield, great crystallinity and scalability. We also report a rational method to manufacture vdW bimetallic MOFs applicable for transition metals with 3d orbitals, from full-filled Zn ($3d^{10}$) to half-filled Mn ($3d^5$) with any two of their combinations. Here there is an exception, we do not consider the Fe metal.

3.2 Materials, Synthesis, and Characterizations

3.2 a Bi-phase synthesis of vdW MOF-2

The materials used were $Zn(NO_3)_2.6H_2O$, $Cu(NO_3)_2.3H_2O$, benzene-1,4-dicarboxylic acid (H_2BDC), pyridine, triethylamine (TEA), hexane, formic acid, isopropanol, and acetone were purchased from Sigma-Aldrich. N,N-dimethylformamide (DMF) and N,N-diethylformamide (DEF) were purchased from Fisher Scientific.

For the bi-phase system, formic acid (0.04 ml), Zn(NO3)2.6H2O (0.18 mmol), pyridine (0.02 ml), and H_2BDC (0.1 mmol) were dissolved in 5 ml of DEF to form the bottom solution. The upper solution was formed by adding TEA (0.07 ml) in 5 ml of hexane. All the components are dissolved first then the bottom solution is slowly injected underneath the upper one. This bi-phase system was sealed in a glass vial and kept at room temperature for 24 hours.

For the growth of vdW MOF-2 on substrates, the selected substrates were held by a Teflon supporter and placed in the DEF phase vertically. The same recipe was also applied to grow Copper-1,4 benzene dicarboxylate (CuBDC) except the $Zn(NO_3)_2.6H_2O$ was replaced with the same mole of $Cu(NO_3)_2.3H_2O$. Samples collected from vials were undergone activation by immersing in 10 ml of acetone for 3 days and drying in vacuum at 120 ℃ for 12 hours. Water intercalation-50 mg of vdW MOF-2 was placed in 10 mL of ultra-pure water for 24 hours. Then, the sample was dried in a fume hood. Pyridine intercalation- 50 mg of HB MOF-2 was placed in 10 mL of pyridine for 24 hours. Then, the sample was dried in a fume hood.

3.2 b Characterizations

The morphologies of vdW MOF-2 and CuBDC were observed with Environmental Scanning Electron Microscope Philips XL30 at a voltage of 10 kV with the assistance of Au sputter coating. Elemental compositions were determined by energy-dispersive X-ray spectroscopy (EDX) which is combined with SEM instrumentation. The Raman spectroscopy measurements were taken using a Renishaw InVia Raman microscope under 100 objective lenses using 488 nm laser as the excitation source, and the laser power was set to 37.5 μW.

3.2 c Results and discussion on the above set of experiments

Achieving Control over Interlayer Hydrogen Bonds versus vdW Forces:

Conventional MOF-2 is a Zinc-1,4 benzene dicarboxylate (ZnBDC) framework consisting of Zn tetrahedral clusters connected by four benzene-1,4-dicarboxylic acid (H_2BDC) via coordination bonds, forming molecular arrangements in 2D landscape.

From Yaghi's research work[8], although these repeated units are constructed along 2D directions, their layers are stacked onto each other tightly by hydrogen bonds. Even common methods such as mechanical exfoliation, polymer-assisted transfer, and liquid phase exfoliation mainly fail to produce large-scale MOF-2 nanosheets with high aspect ratios. In figure 3-1 a, depicts the conventional growth in which the uniform solution (shown as blue liquid) consists of dimethylformamide (DMF), water molecules (pink branches), ligand–terephthalic acid (gray bar), and zinc cluster (blue dots), and this synthesis involving these precursors simply produces strongly coupled sheets with low aspect ratio that have overall bulk appearance (labeled HB MOF-2).

We have developed a novel dimension-controllable growth method in order to achieve 2D vdW MOF nanosheets that are weakly coupled through vdW forces as shown in Figure 3-1b. In this method, the goal is to minimize interlayer (out-of-plane) growth and reduce interlayer coupling strength to yield ultrathin vdW layered MOF-2 sheets, while controlling the in-plane (sheet) growth rate. Hypothesis made for achieving vdW layers relies on replacing precursor H_2O that is used in HB MOF-2 synthesis with pyridine molecules along with rate controlling TEA and formic acid agents. The role of pyridine is to replace interlayer hydrogen(h) bonding or other weak chemical bonds to achieve high aspect ratio (large size 2D sheets) with high crystallinity. In MOF-2, Zn sits in a square-pyramid coordination geometry with a coordination number at 5, in which the deprotonated ligands (BDC) occupy four coordination sites and the remaining site is occupied by H_2O. Latter site is the origin for the formation of hydrogen bonding across the layers which in return creates strong coupling and thus producing huge chunks of crystals as clearly shown in Figure 3-1a.

To prevent the formation of hydrogen bonds and to convert the interlayer bonding from hydrogen to vdW, our method substitutes $_{H2O}$ with pyridine molecules (C_5H_5N depicted in red in Figure 3-1b), which has energetically favorable binding energies to Zn (0.92 eV) in comparison to H_2O–Zn bonding (0.51 eV). In parallel, our process utilizes TEA and formic acid agents that have been found to be necessary for high yield synthesis of vdW MOF-2 by controlling the reaction speeds.[101]

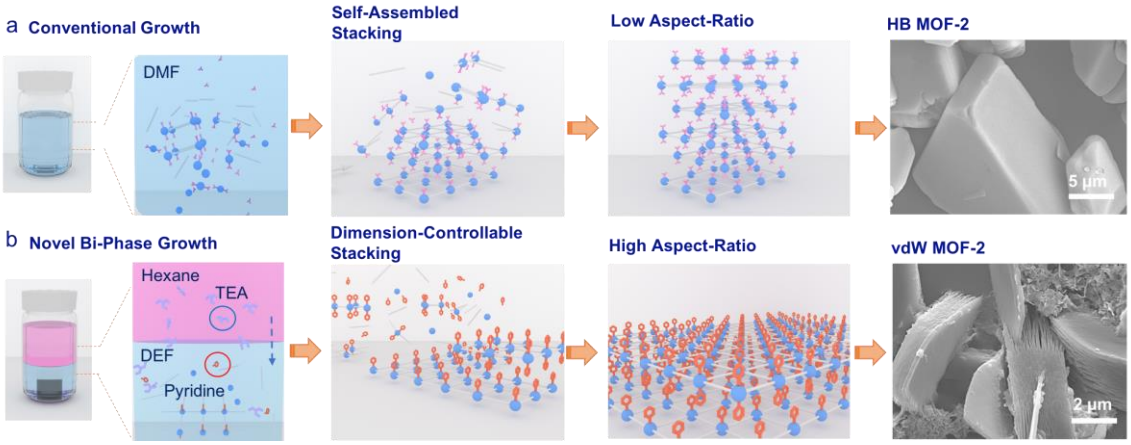

Figure 3-1 Synthesis routes toward industrially scalable 2D MOF. a) Schematic description of synthesis routes utilized in conventional growth yielding traditional HB MOF-2; b) schematic description of HB MOF-2.

3.3 Synthesis of vdW-MOF-2 by Water with Pyridine Replacement Route

The reaction setup is a bi-phase synthesis which includes 1) the upper phase (pink region in Figure 3-1b) consisting of hexane mixed with TEA (which is displayed as branches in light purple highlighted in red circle) and 2) the bottom phase consists of dimethylformamide (DEF) dissolved with metal precursors (M = Zn and Cu) and the ligand (H_2BDC), as well as pyridine (highlighted in red circle).

3.3 a Results and Discussions

The addition of pyridine in the bottom phase was found to be highly effective in producing highly lamellar vdW MOF-2, as shown in Figure 3-1b, this is due to the replacement of hydrogen bonds with pyridine molecules around metal sites and reduction of interlayer forces. When replaced by pyridine, it effectively reduces the hydrogen bond nature, but increases the interlayer separation by linking large pyridine molecule to these metal sites and sustains vdW interactions.[101]

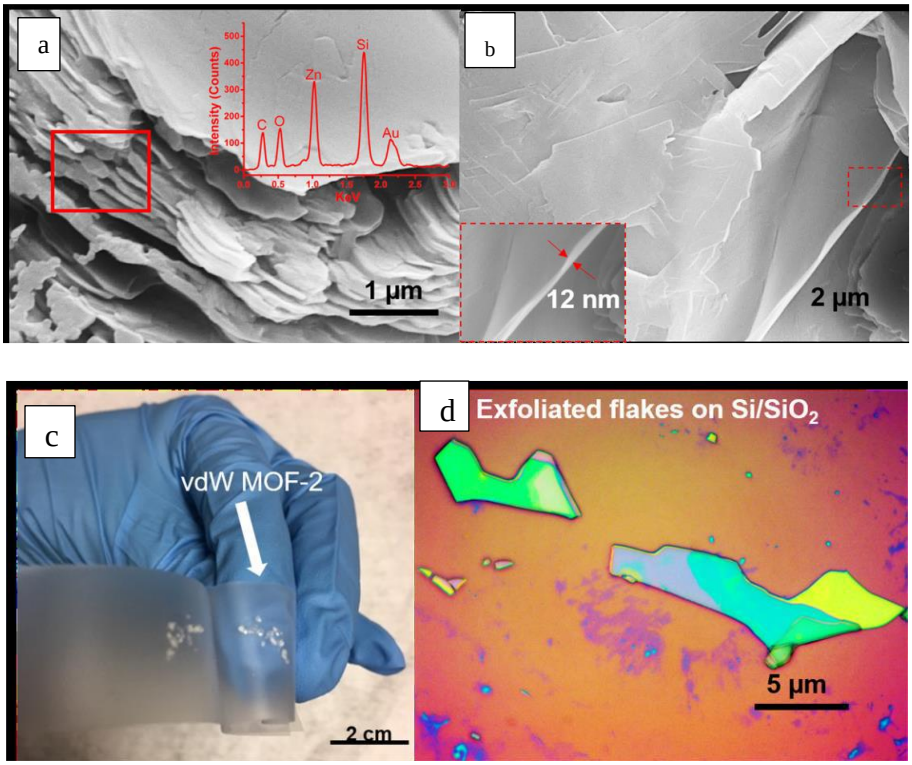

Figure 3-2 Growth and morphology of vdW MOF-2. vdW MOF-2 sheets appear (a)lamellar/layered, exhibit (b)smooth surfaces with thickness at most 10 nm c) Large crystals of vdW MOF2 can be attained by Scotch tape method d) Optical image of the exfoliated crystal

The elemental composition of vdW MOF-2 is confirmed by the corresponding energy-dispersive X-ray spectroscopy (EDX) (Figure 3-2a), the silicon and partial oxygen contribution comes from the underlying Si/SiO2 solid substrates.

The bi-phase method can be used for the synthesis of bulk vdW MOF-2 crystals (Figure3-2c) which is easily collected at the bottom of the reaction vial or in the form of thin film which can be easily deposited onto any arbitrary substrate. Bulk vdW MOF-2 crystals easily reach gram scales and can even be scaled to larger volumes by simply increasing the overall volume of the precursors. Synthesized bulk vdW MOF-2 shows striking similarities to lamellar h-BN, graphite, or MoS2 crystals in which they can easily be exfoliated using Scotch tape (Figure 3-2d) to yield monolayers. Even low-magnification SEM images are sufficient to observe extremely thin lamellar sheets (≈10 nm) which comfortably reach up to 10 s of μm and lateral sizes (Figure 3-2 b, c). Such obtained MOF-2 with extremely high aspect ratio (>103) is a direct evidence of the dimension-controllable stacking behavior.[101]

Comparison between theoretical XRD patterns (black solid line) and experimental datasets acquired from synthesized vdW MOF-2 (red solid lines) are shown in Figure 3-3b. Closer look at the calculated and experimental XRD patterns of vdW MOF-2 shows confirmed 00*l* reflections related to reflections from adjacent vdW layers, and most of the prominent peaks can be closely matched to those simulated ones. 2^{o} values are as close as $\sim 0.4^{0}$. We also note that vdW MOF-2 is indeed lamellar in nature as evidenced by DFT binding energy calculations. Further structural confirmation was obtained by comparing calculated vibrational spectrum (simulated Raman spectrum) to experimental Raman spectrum in Figure 3-3f. Black solid line in the same figure represents a simulated Raman spectrum coming from DFT calculations.

To demonstrate the role of pyridine and conversion between HB and vdW MOF-2 structures, immersed vdW MOF-2 sheets under ultrapure H_2O for 24 h. The results showed that vdW MOF-2 structure successfully transitions from vdW like to HB like (Figure 3-3d) which means that H_2O molecules effectively diffuse between the layers and replace pyridine groups with H_2O. Also noted that large crystal structure changes are highly unlikely since the process itself is limited to room temperature. This process also offered evidence that pyridine molecules originally sit where hydrogen bonds are positioned since interaction with H_2O simply reduces vdW into HB MOF-2 (see schematic in Figure 3-3d and XRD datasets in Figure 3-3e). Reported this chemical reaction is unidirectional since drying transformed. HB MOF-2 does not reverse the structure (Figure 3-3 d).

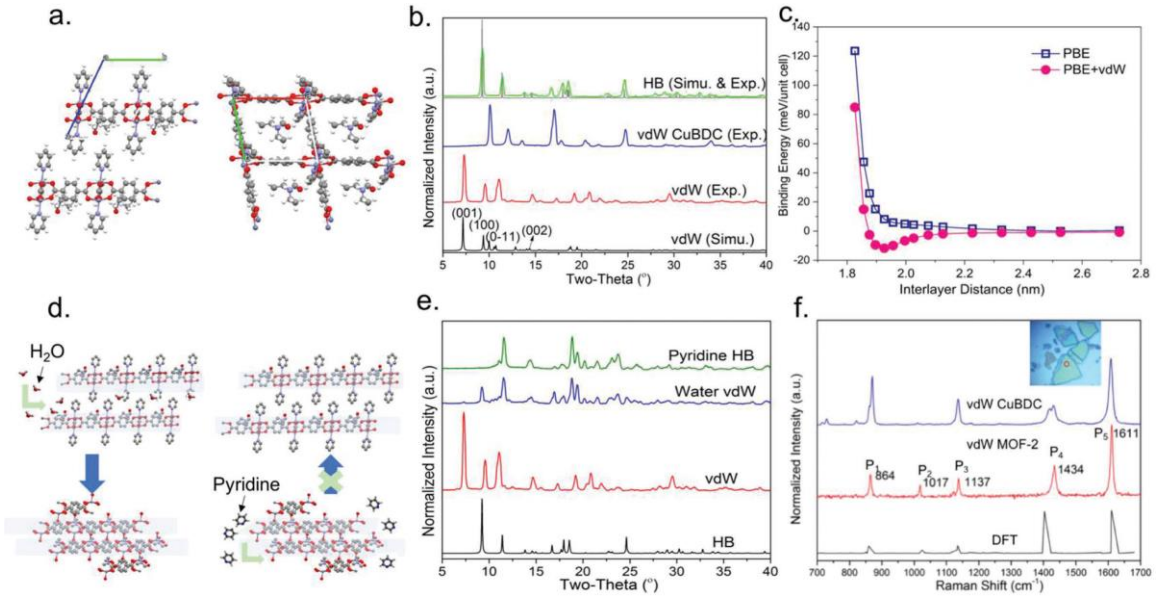

Figure 3-3 a) Refined structure of vdW MOF-2; b) powder XRD patterns of HB MOF-2 (experimental and simulated) and vdW MOF-2 (experimental and simulated) as well as vdW Cu(BDC); c) interlayer binding energy calculated by DFT; d,e) vdW MOF-2 samples soaked under water under irreversible transformation from vdW to HB due to pyridine–water replacement mechanism. f) Micro-Raman spectra of vdW MOF-2 (ZnBDC), as well as DFT simulation results, respectively, and inserted optical images of MOF-2 and CuBDC with white spots show the locations where micro-Raman spectra are measured. Reproduced with permission from Yuixa Shen et, al[101]

Similarly, we expand our explanations to the results obtained above to Nickel 1,4 benzene dicarboxylate (NiBDC) and Cobalt-1,4 benzene dicarboxylate (CoBDC) MOFs.

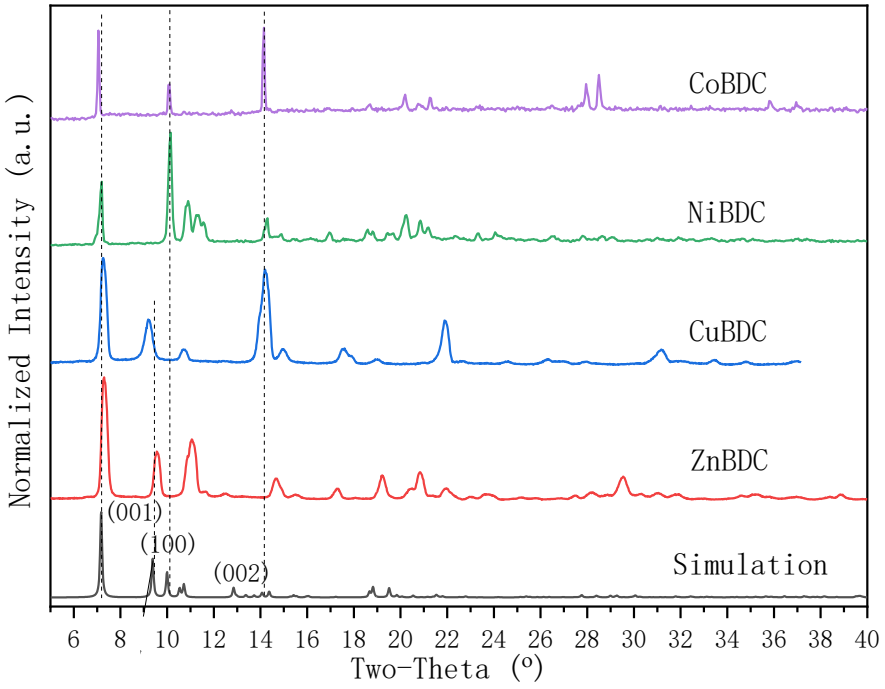

Figure 3-4 XRD pattern of the MOFs.

These crystals exhibit similar XRD patterns (Figure 3-4). The purple color corresponds to the diffraction pattern of CoBDC MOF and green color corresponds to the diffraction pattern of NiBDC. Similarly, blue and red color corresponds to the diffraction pattern of CuBDC and MOF-2 (ZnBDC) respectively. According to simulation results of all the crystals, their layers are stacking along (001) direction. The calculated d-spacing is 1.2 nm.

From the optical images shown in Figure 3-4a MOFs are clearly seen as layered. DFT calculations for NiBDC and CoBDC MOFs are based on MOF-2(ZnBDC) vdW which are indeed lamellar in nature and are similar to MOF-2 as evidenced by DFT binding energy calculations shown in black (Figure 3-4 b).

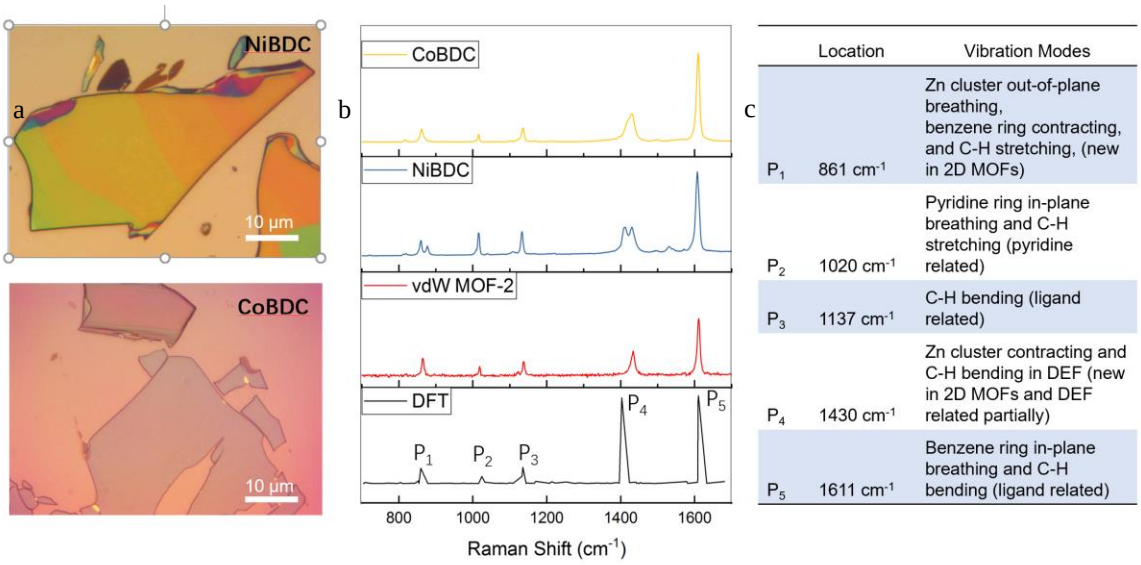

Figure 3-5 a) Optical images of top NiBDC and bottom CoBDC; b) Raman data; c) Table showing atomic vibrations

Typical Raman spectrum collected from MOF-2 sheets exhibited five prominent peaks (Figure 3-5 b) with low FWHM (≈6 cm−1), located at 864, 1017, 1137, 1434, and 1611 cm^{-1} and marked as P1, P2, P3, P4, and P5, respectively are explained in the table in Figure 3-5c.From Raman, this comparison says Ni and Co have similar lattice vibrations and after calculating FWHM (6-10 cm^{-1}) it confirms good crystallinity.

The above discussion leads our project to proceed further in trying the synthesis of MOF alloys. Metals were selected according to their coordination number, electronegativity and the role of pyridine to prevent the interplanar hydrogen bonding. Capping effect of pyridine in 2D MOF alloys has two-fold contributions: 1) promote layers are stacking along out-of-plane direction, which is consistent with our previous results; 2) improve the crystallinity by forming partially bonded metal species acted as unidental ligands.

3.4 Synthesis of MOF alloys

3.4 a Single-phase synthesis of MOF alloys

The materials used were $ZnCl_2$, $Cu(NO_3)_2.3H_2O$, $NiCl_2.6H_2O$, $MnCl_2.4H_2O$, Cobalt chloride, Terephthalic acid (H_2BDC), pyridine, acetone that were purchased from Sigma-Aldrich without further purification. N,N-dimethylformamide (DMF) were purchased from Fisher Scientific. Alloys of metals were in the combination of Nickel-Zinc (Ni-Zn), Copper-Zinc (Cu-Zn), Cobalt-Zinc (Co-Zn) and Manganese-Zinc (Mn-Zn) corresponding to different molar ratios of the metals. The ligand molar ratio was kept constant throughout. Pyridine was added to the solution of metals and ligand that were sonicated for proper mixing. The sonicated solution was put inside the autoclave and placed inside the oven for crystal growth with a temperature of 120 degree Celsius for 24h. After the growth, the crystals were cleaned with Acetone.

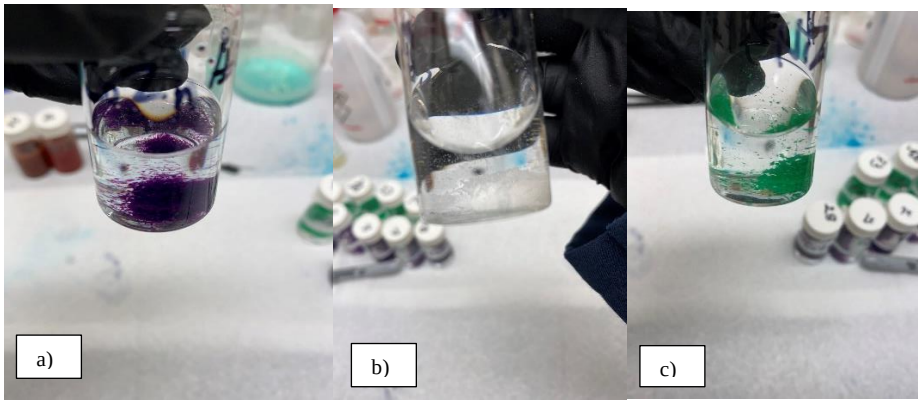

Figure 3-6 MOF alloy crystals after crystal growth. a) Cu-Zn BDC crystals, b) Mn-Zn BDC crystals and c) Ni-Zn BDC crystals.

Figure 3-6 above shows the different alloys synthesized by a single-phase system. There was clear crystal growth for Copper-Zinc BDC with blue crystals and for Nickel-Zinc BDC which gave us beautiful green crystal. Manganese- Zinc BDC alloy was flakier in texture compared to the rest of the crystals and it was greyish-white in color.

3.4 b Results and Discussion

We report an analogous method to synthesize vdW bimetallic MOFs using single phase with capping agent pyridine and is applicable for transition metals with 3d orbitals, from full-filled Zn ($3d^{10}$) to half-filled Mn ($3d^5$) with any two of their combinations (Figure 3-7 d). As such, two different metal ions are named as "M^1" and "M^2". With the connection via ligands benzene-1,4-dicarboxylic acid (BDC) and capping agent- pyridine, the constructed vdW MOF alloys is denoted as "$M^1_xM^2_{1-x}$BDC" (Figure 3-7 a).

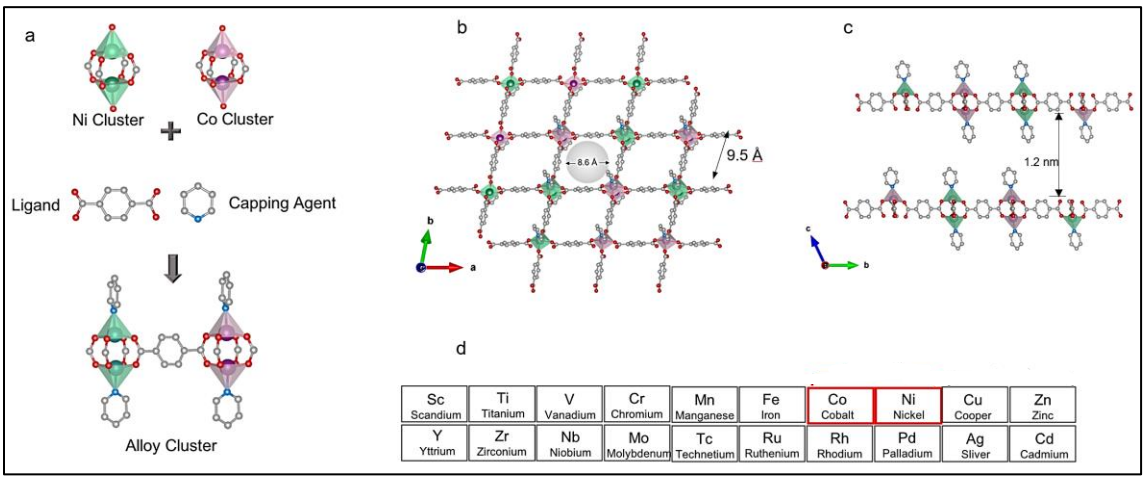

Figure 3-7 Schematic structure of 2D vdW MOF alloys ($M^1_xM^2_{1-x}$BDC) a) the basic building units in $M^1_xM^2_{1-x}$BDC; b) top view of obtained $M^1_xM^2_{1-x}$BDC with randomly arranged M^1 and M^2 clusters; c) side view of layer-to-layer stacking via vdW force; d) involved metal types in partial periodic elemental table.

Its crystalline in-plane structure consists of M^1 or M^2 clusters with a square coordination geometry interconnected by BDC anions. Pyridine molecules attached on metal sites run along the stacking direction (Figure 3-7 b). From the side view (Figure 3-7 c), these vdW layers are stacking along (*001*) direction with a spacing distance of 1.2 nm. These crystallography features are indicated in powder X-ray Diffraction patterns which is explained later in this chapter.

SEM images of the synthesized alloys

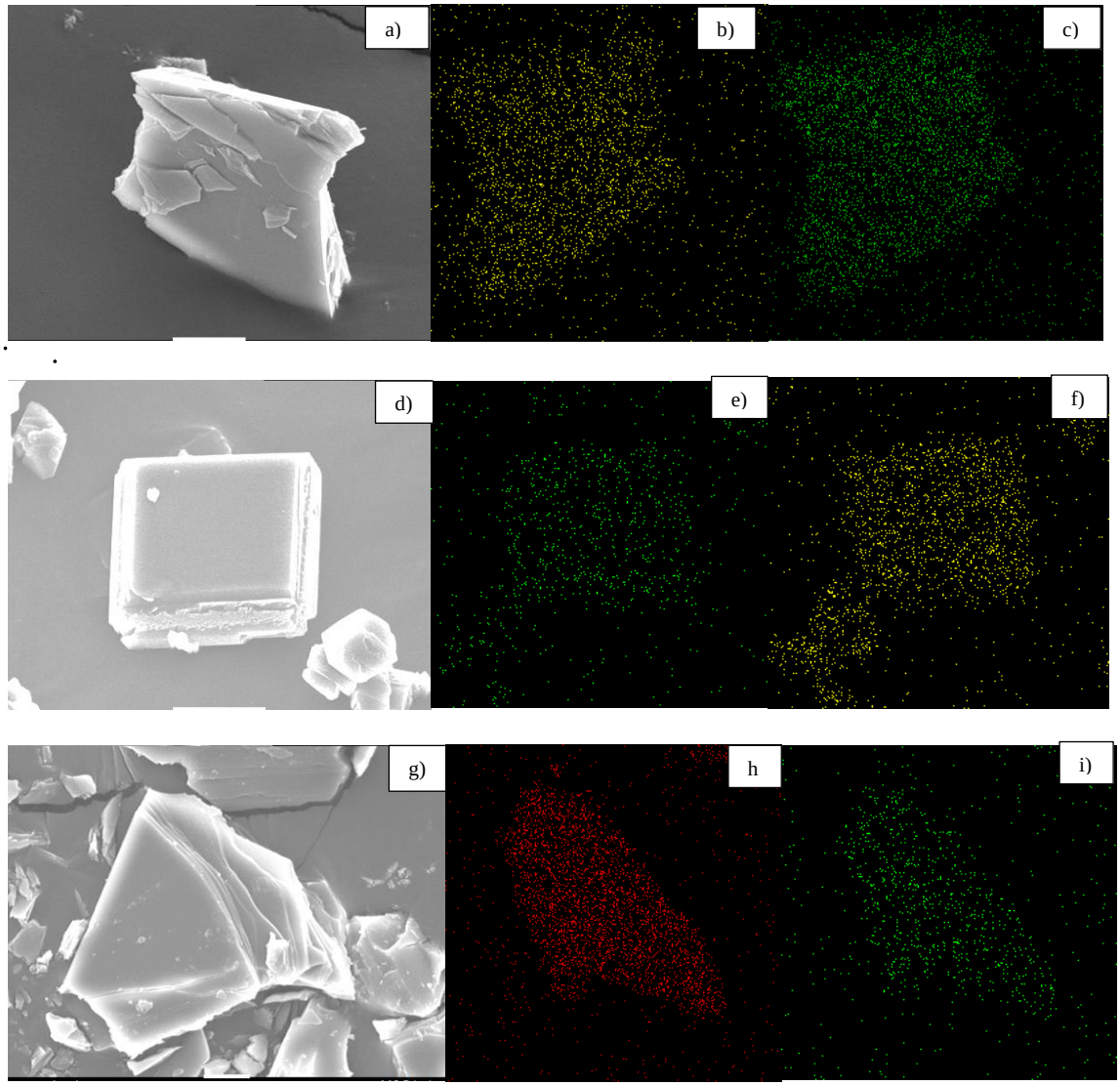

Figure 3-8 a) SEM image of Ni-Zn BDC alloy; b) and c) shows the EDS mapping images of Ni and Zn of the alloy respectively. Similarly, d) SEM image of Cu-Zn BDC alloy; e) and f) shows the EDS mapping images of Zn and Cu of the alloy respectively. And g) SEM image of Co-Zn BDC alloy; h) and i) shows the EDS mapping images of Co and Zn alloys respectively.

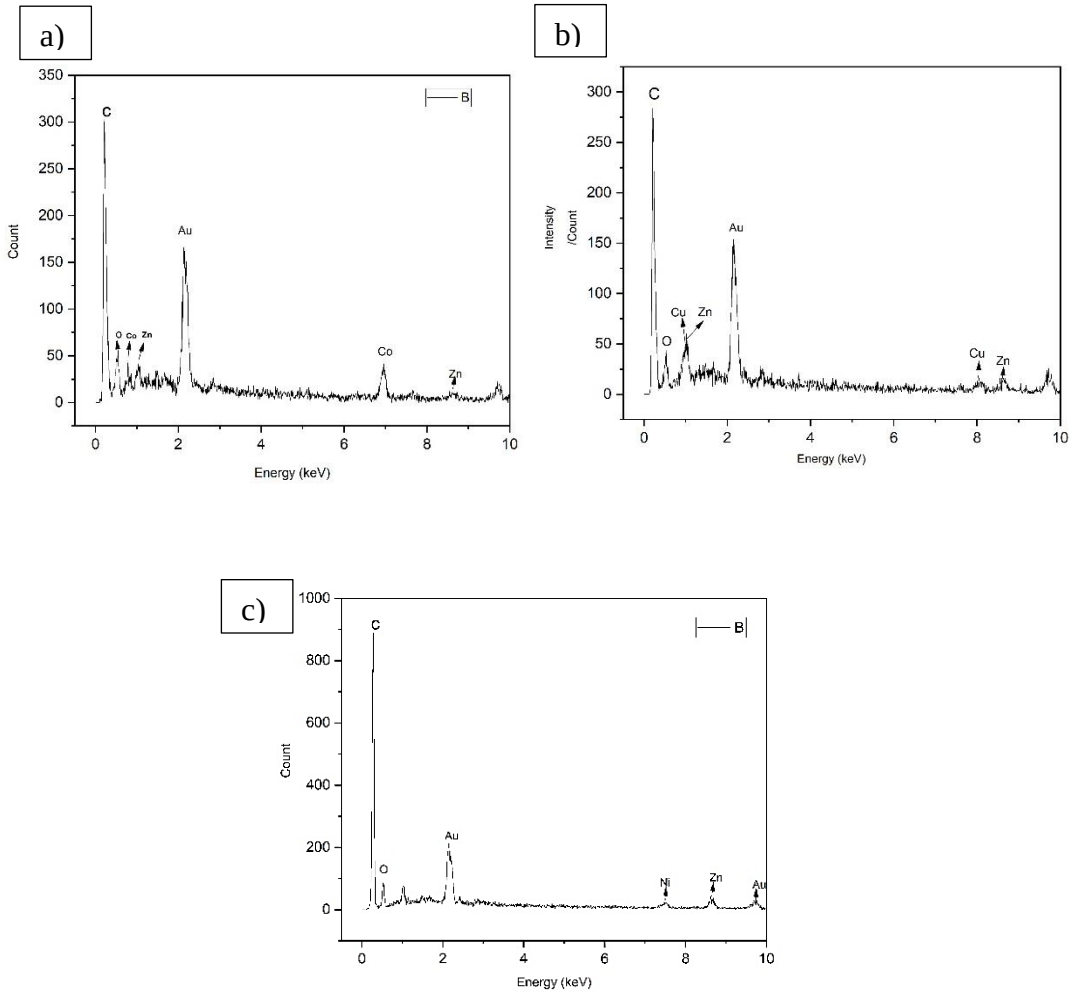

Figure 3-9 Elemental composition detected by Electron dispersive spectroscopy: a) Co-Zn BDC alloy, b) Cu-Zn BDC alloy and c) Ni-Zn BDC alloy.

SEM images (Figure 3-8) detail the layered morphology of the MOF alloys. In the given EDS mapping, we can see that the metals are really in the MOF alloy structures and metals are uniformly dispersed (Figure 3-8). The SEM images and EDS data (Figure 3-9) confirms the layered morphology and the presence of both the metals in the crystal structures.

In addition, the same synthesis methodology can be successfully extended to produce high-aspect-ratio sheet crystals of a variety of layered MOF structures via substitution of Ni/Co for alternative metal pairs, e.g. M^1/M^2= Zn/Cu, Zn/Ni, Zn/Co Cu/Ni and Cu/Co. Interestingly, similar to $Ni_xCo_{1-x}BDC$, a competitive growth feature has been identified in all these MOF alloys.

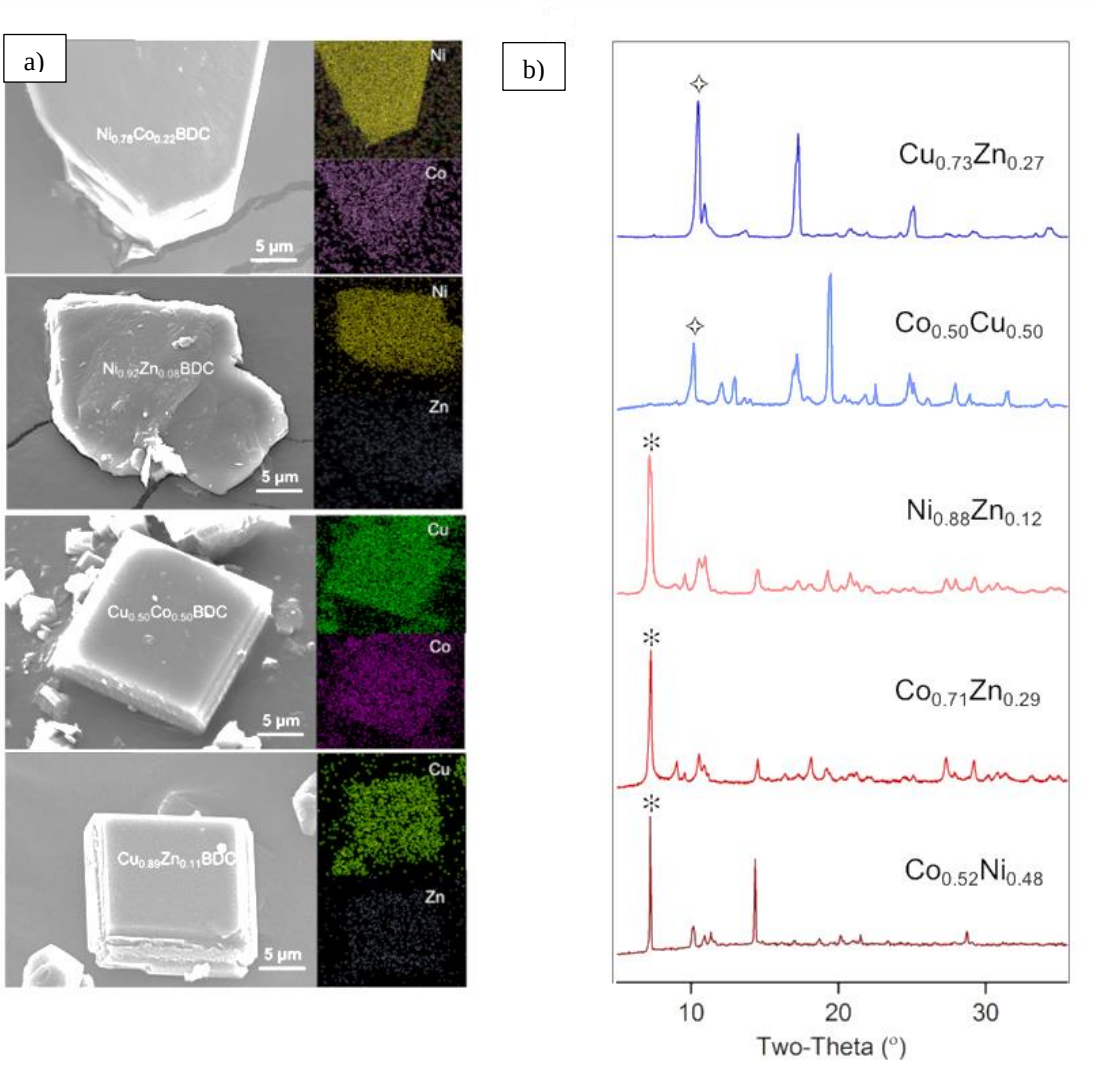

Figure 3-10 a) 2D MOF alloys by substituting M^1/M^2 = Zn/Cu, Zn/Ni, Cu/Ni and Cu/Co. SEM and EDS mapping images suggest their lamellar morphology and uniform composition; b) XRD comparison among M^1M^2BDC MOF alloys, with M^1M^2= CoNi, CoZn, NiZn, CoCu and CoZn. Predominant peaks are marked as special characters.

Resulting 2D MOF alloys, $Ni_{0.78}Co_{0.22}BDC$, $Ni_{0.92}Zn_{0.08}BDC$, $Cu_{0.50}Co_{0.50}BDC$, and $Cu_{0.89}Zn_{0.11}BDC$ are all exhibiting vdW stacking morphology. Typical SEM and EDS mapping are demonstrated in Figure 3-10**.** To investigate their crystal information, we performed powder XRD of these solid products and compared $Ni_{0.52}Co_{0.48}BDC$ to the collected dataset (Figure 3-10 b). It has been found that in the combinations of Co/Ni, Co/Zn and Ni/Zn, the predominant peaks of (001) and (002) are all observed (marked as stars).

The similarity in these diffraction patterns suggested consistent crystal structure in the alloys. However, in the presence of Cu, like $Co_{0.50}Cu_{0.50}BDC$ and $Cu_{0.73}Zn_{0.27}BDC$, the preferred diffraction planes are tuned in (100) and (200), located at 10.5^{o} and 19.8^{o} respectively. In addition, the changed orientation is not caused by Cu solely. We have reported that CuBDC has dominant XRD peaks of (001) and (002) similarly to that in ZnBDC. Therefore, we argue that such phase transition is a result of collective impact between Cu and Co or Cu and Zn.

Apart from the competitive growth discussed above, the capping agent (pyridine) used in the system is critical for the vdW morphology formation in alloys. In our previous reports, it has been found that the use of pyridine is effective in producing highly lamellar MBDC (M= Zn, Cu and Mn) by terminating the out-of-plane metal sites (or reduce the available bonding). While, the capping effect is still valid in the bimetallic alloyed systems. Taking Ni/Co as an example again, a series of control experiments were performed on $Ni_xCo_{1-x}BDC$ with/without pyridine (Figure 3-11).

Their morphological comparison by SEM indicate that the utilize of pyridine promotes the vdW layered morphology and smooth surface. In the case of pyridine- absent, $Ni_{0.52}Co_{0.48}$BDC clearly display a bulky and rough appearance. In XRD image (Figure 3-11), X-ray diffraction of $Ni_{0.52}Co_{0.48}$BDC with pyridine showed limited reflections which can be indexed as *(001)* and *(002)* at 7.8° and 15.6° respectively. These intense diffractions indicate a strong preferential orientation, and lattice are stacking along *(00l)* directions, corresponding to a spacing distance of 1.2 nm. Similar to our previously reported vdW MOF-2 (ZnBDC), as-grown $Ni_{0.52}Co_{0.48}$BDC possess classic vdW nature.

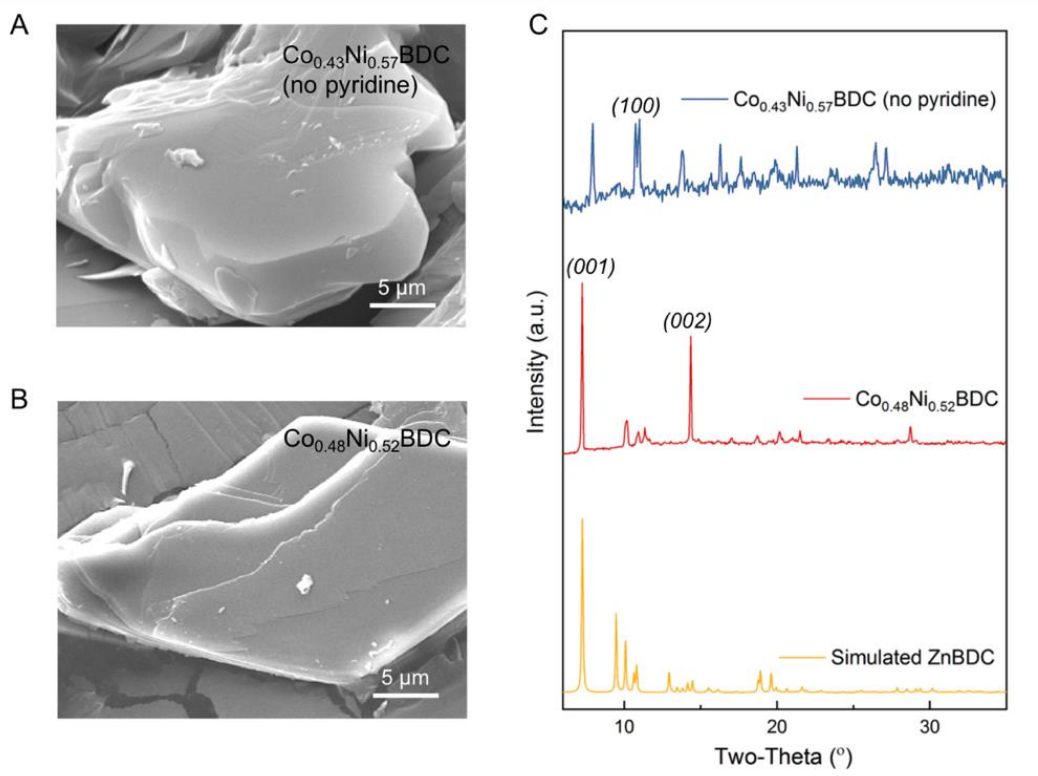

Figure 3-11 Control experiments of CoNiBDC alloys in terms of the roles of pyridine.

Deriving alloying atomically is an intensively applied technology in inorganic materials to adjust their properties. The synthesis of highly ordered alloys with great structural integrity remains challenging because of the disturbed chemical environment orienting from the guest species possessing different chemical reactivity to the host atom.

This kind of problem is more evident in 2D MOFs in which atoms are bonded mainly via weak coordination bonds. During the synthesis of 2D MOF alloys, it was found that the two different metal ions compete with each other in their coordination reaction to ligand BDC.

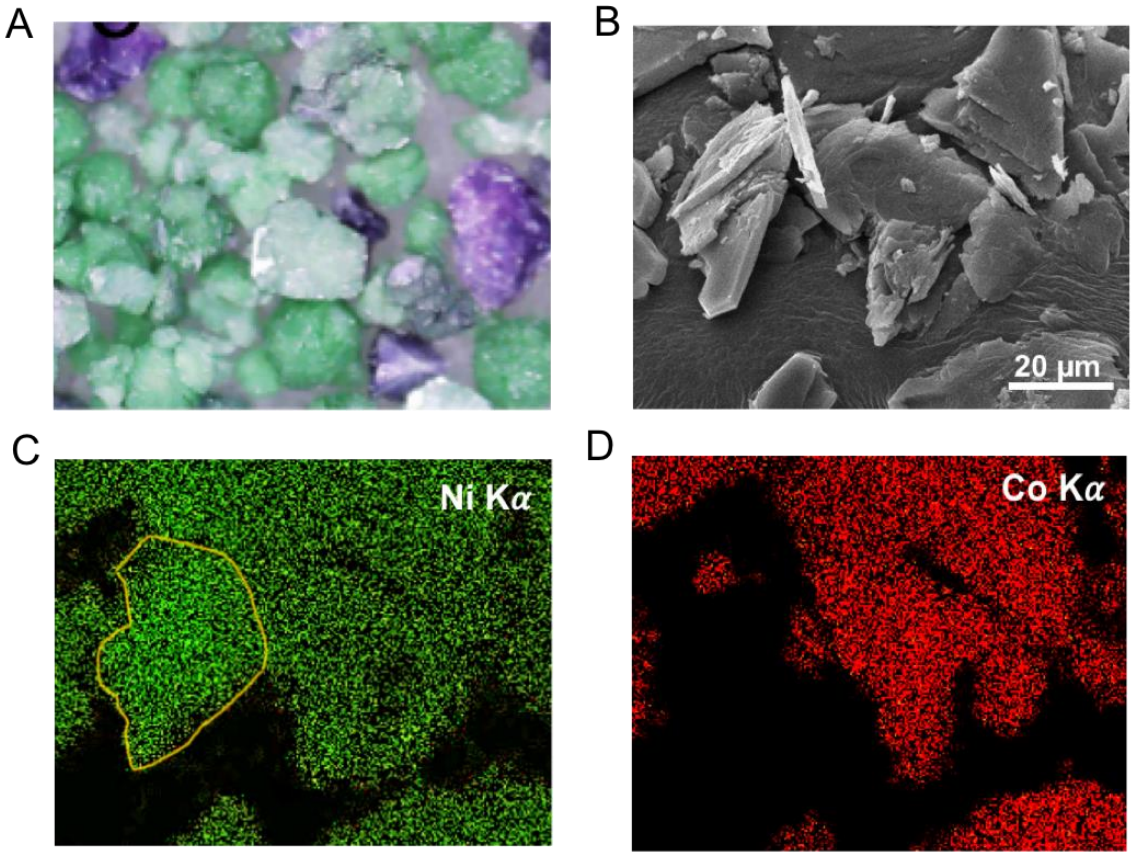

Figure 3-12 Phase separated product with the starting precursor $NiCl_2/CoCl_2$=0.5/0.5 in molar.

For example in case of Co-NiBDC, taking M^1= Co and M^2= Ni with the starting molar ratio of Co/Ni = 0.5/0.5 in their respectively chloride precursors, the products formed were a mixture of NiBDC (majority in green) and few $Co_{0.21}Ni_{0.79}$BDC alloys (purple) as shown in Figure 3-12 A.

This phase-separated production is confirmed in EDS mapping of NiKα and CoKα correspondingly (Figure 3-12 C, D). We believe that the presence of Ni restricts the Co-O bonding formation with ligands. Systematic experiments proved that in the pair of Ni/Co, Ni ions exhibit stronger competition with respect to Co during the formation of MOF alloy Ni_xCo_{1-x}BDC. As a result, not all the Co cations from its precursor are able to participate in the formation of alloy structure.

Successfully synthesized 2D MOF alloys by single-phase method. Pyridine being the capping effect is still valid in the bimetallic alloyed systems. During the experimentation Co-NiBDC came across to be as a phase separated product. This result gives rise to future analysis on controlled growth over Co-NiBDC.

The controllable synthesis of 2D MOF alloys with tailorable metal clusters was achieved and this merits future studies on their optical properties. We also need to investigate the contributions of different metal clusters on the band gaps of MOF alloys.

CHAPTER 4

OVERVIEW ON INTERCALATION CHEMISTRY OF 2D MOFs AND THEIR ALLOYS

4.1 Bromine intercalation on 2D MOFs and their alloys.

The intercalation chemistry studies has been heavily used to understand the change in the band gap as well as electronic conductivity of vdW layered inorganic materials such as graphite/graphene and transition-metal dichalcogenides.[100,106-107] However, this method is not so straightforward for MOFs or other polymeric materials owing to their strong interlayer coupling.[100,108] During the Br_2 treatment experiment, lamellar and bulk crystals of CoBDC, Ni-CoBDC and NiBDC were spread flat at the bottom of glass plates separately as shown in Figure 4-1a. The following experiments were performed in a chemical fume hood with proper personal safety. First, bromine liquid (2 mL) was dropped in another glass container and inserted into a large beaker with its lid open. Both bulk and lamellar materials were placed in this beaker and sealed using parafilm to expose bromine gas to materials. Because bromine has a high vapor pressure at room temperature, the bromine gas reached its saturated vapor pressure within 30 min and the entire sealed beaker gradually fills up with gas from light orange to dark red (illustrated by the inset in Figure 4-1b). Once the bromine treatment was completed (for three hours), MOFs were collected and characterized immediately.

a

Bromine treatment to MOFs and MOF alloy

CoBDC | Ni-CoBDC | NiBDC

b

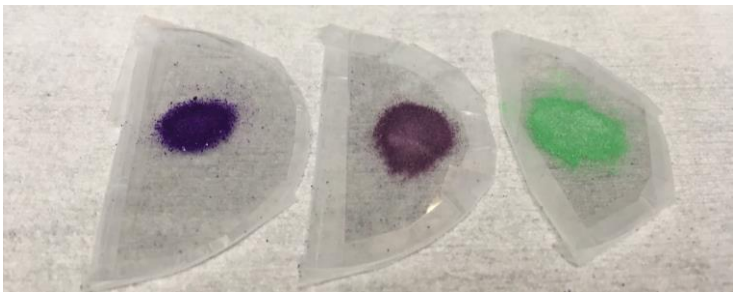

After Br2 treatement

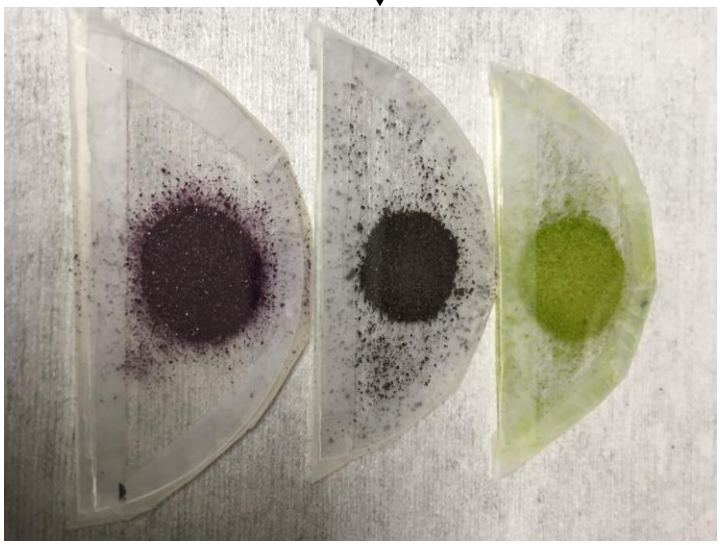

CoBDC | Ni-CoBDC | NiBDC

Figure 4-1 a) Bromine treatment to MOFs and MOF alloy, b) Color change of the crystals before and after the bromine treatment.

4.2 Characterization on the Bromine treated MOFs and their alloy

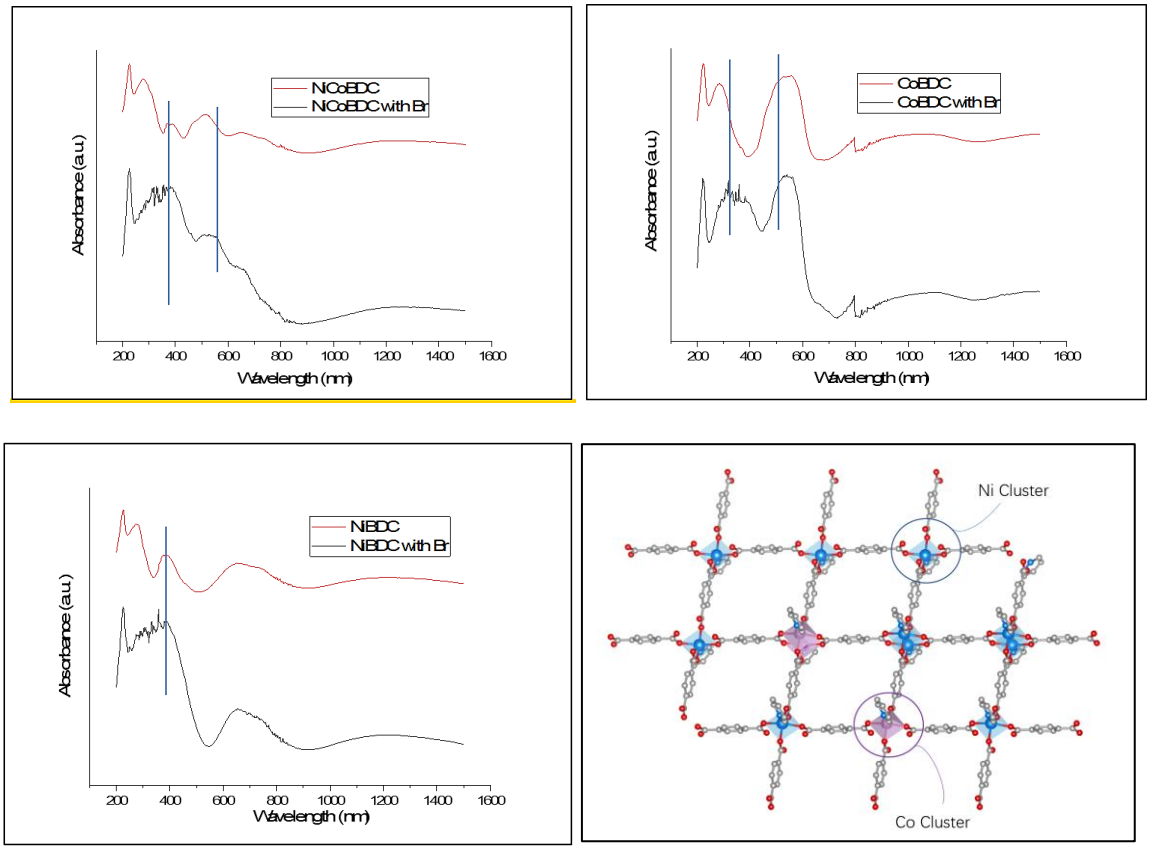

Figure 4-2 Comparison of Optical absorption Spectra of the crystals before and after Bromine treatment. a) CoBDC, b) NiCoBDC and c) NiBDC; d)Schematic structure of NiCoBDcC alloy

After Br treatment, we can clearly see that optical absorption spectra changed for the crystals. After Bromine intercalation the optical spectrum changed slightly for NiBDC and CoBDC whereas for alloy it changed significantly to a longer wavelength. Especially for Ni-CoBDC, its main peaks shift to longer wavelength, which indicates reduced band gap.This interestingly is similar to the studies of band gap engineering using intercalation chemistry in layered MnBDC [100].

The above absorption spectra explain that layered MOFs and MOF alloy both exhibit red-shift in their band gaps which leads us to attribute that large band-gap variation to the layered nature of NiBDC, CoBDC and Ni-CoBDC sheets enabled bromine gas to intercalate between the layers. But there is a significant red-shift in the band gap of MOF alloy However, the fundamental origin of such a redshift in the optical gap still remains unknown owing to complexities in calculating the electronic band structure of Br intercalated MOF alloy layers. We argue that the intercalated Br atoms must have an overall effect to increase the energy of valence band maxima (VBM) or reduce the energy of conduction band minima (CBM) level to cause red-shift in the band gap [100]. Though the nature of large red-shift in their band gap values remain unknown but merit future studies, our results clearly demonstrate that the layered morphology facilitates the diffusion of bromine between MOFs and MOF alloy layers. Bromine intercalation results can be further used to study the band gap engineering in these synthesized exciting MOF crystals and their alloys.

CHAPTER 5

CONCLUSION AND FUTURE DIRECTIONS

5.1 Conclusion

In this thesis work, a new approach is derived in studying the competitive growths of 2D metal-organic frameworks and their alloy systems. A novel method referred to as bi-phase synthesis was adopted here to promote the formation of ultrathin vdW MOF nanosheets such ZnBDC and CuBDC. The employment of this bi-phase synthesis system is for the production of high quality and high yield of 2D MOF nanosheets at the same time. Overall findings until date on synthesis of highly crystalline 2D MOFs and their alloys are anticipated to open up new avenues toward large-scale synthesis of vdW MOFs by offering ways to manipulate interlayer coupling strength and reaction rates and offer fundamental insights into their thickness-dependent properties

It is already demonstrated that a scalable and reproducible bi-phase synthesis method for highly crystalline and great quality production of vdW MOFs sheets. Also, replacing water molecules with pyridine has been identified as the primary factor sustaining perfectly layered vdW MOF sheets. First this study reported hydrogen bonds can be substituted by capping agent pyridine which forms an effective route to form vdW stacked layers in 2D MOF mBDC (m= Zn and Cu). The addition of pyridine can promote the formation of 2D MOF structures when a metal ion has a more complex possible coordination geometry. Demonstrated the addition of pyridine in the synthesis can promote the anisotropic growth of both ZnBDC and CuBDC. This study was extended to validate how this strategy behaves at the presence of two different metal ions.

We report a rational method to synthesize vdW bimetallic MOFs using single phase with capping agent pyridine and is applicable for transition metals with 3d orbitals, from full-filled Zn ($3d^{10}$) to half-filled Mn ($3d^5$) with any two of their combinations. There was successful alloying of Cu-Zn BDC Ni-ZnBDC and Co-ZN BDC alloys. Ni or Co metal atoms are different from Zn and Cu atoms due to their partially un-occupied d orbitals which may induce electron transfer and benefit the redox reactions such as it can be applied in band gap engineering and catalysis. The 2D structure was successfully achieved under the addition of just pyridine and was synthesized in a single phase. The capping agent (pyridine) used in the system is critical for the vdW morphology formation in alloys.

The classic vdW nature enables us to perform Bromine intercalation on MOFs for the first time. Owing to large lateral size, layer-by layer stacking, and high crystallinity in the MOFs and their alloys we were able to utilize bromine intercalation to investigate the changes in the band gap with intercalation chemistry. Bromine intercalation results indicate the incorporation of Br changes the optical properties of 2D MOFs clearly. Their optical band gaps are reduced accordingly.

5.2 Future Directions

Synthesizing MOF alloys using different metal-metal combinations to produce new frameworks is a challenging yet fruitful work if successful. Manganese and Iron MOFs are quite challenging to obtain defect free MOF films, but it's a great start to study and produce these new materials. The beautiful and best properties of the 2D MOF frameworks can be achieved if they are explored keenly.

Hence, systematic investigation on 2D MOF alloys with controllable metal ratios should be of keen interest to produce highly crystalline and defect free 2D MOF alloy film. In future work, new polymer matrix will be combined with 2D MOFs to generate mixed matrix membranes for different gas separations. We should also focus on producing Fe-Zn alloys and various combinations of metal-metal BDC to explore its application on catalysis. Combine with theoretical collaboration, understand the bandgap engineering after Br treatment.

REFERENCES

1. M. Zeng, Y. Xiao, J. Liu, K. Yang, and L. Fu, Exploring Two-Dimensional Materials toward the Next-Generation Circuits: From Monomer Design to Assembly Control *Chem. Rev*. 118, 6236 (2018).

2. S. Manzeli, D. Ovchinnikov, D. Pasquier, O. V. Yazyev, and A. Kis, 2D transition metal dichalcogenides. *Nat. Rev*. *Mater*. 2, 17033 (2017).

3. K. Zhang, Y. Feng, F. Wang, Z. Yang, and J. Wang, Two dimensional hexagonal boron nitride (2D-hBN): synthesis, properties and applications *J. Mater. Chem*. C 5,11992 (2017).

4. M. Khazaei, A. Mishra, N. S. Venkataramanan, A. K. Singh, and S. Yunoki, Curr. Opin. Distinguishing electronic contributions of surface and sub-surface transition metal atoms in Ti-based MXenes, *Solid State Mater. Sci*. 23, 164 (2020).

5. H. An, T. Habib, S. Shah, H. Gao, M. Radovic, M. J. Green, and J. L.Lutkenhaus, Surface-agnostic highly stretchable and bendable conductive MXene multilayers *Sci. Adv.* 4, eaaq0118 (2018).

6. P. Lakhe, E. M. Prehn, T. Habib, J. L. Lutkenhaus, M. Radovic, M. S.Mannan, and M. J. Green, Process Safety Analysis for Ti3C2Tx MXene Synthesis and Processing *Ind. Eng. Chem*. Res. 58, 1570 (2019).

7. H. An, T. Habib, S. Shah, H. Gao, A. Patel, I. Echols, X. Zhao, M. Radovic, M. J. Green, and J. L. Lutkenhaus, Water Sorption in MXene/Polyelectrolyte Multilayers for Ultrafast Humidity Sensing *ACS Appl. Nano Mater*. 2, 948 (2019).

8. T. Habib, X. Zhao, S. A. Shah, Y. Chen, W. Sun, H. An, J. L. Lutkenhaus, M.Radovic, and M. J. Green, Oxidation stability of Ti3C2Tx MXene nanosheets in solvents and composite films *npj 2D Mater*. Appl. 3, 8 (2019).

9. Y. Chen, Y. Sun, J. Peng, J. Tang, K. Zheng, and Z. Liang, 2D Ruddlesden–Popper Perovskites for Optoelectronics *Adv. Mater*. 30,1703487 (2018).

10. M. Tran, K. Kline, Y. Qin, Y. Shen, M. D. Green, S. Tongay, 2D coordination polymers: Design guidelines and materials perspective *Appl. Phys*. Rev. 6, 041311(2019)

11. C. E. Boott, A. Nazemi, and I. Manners, Synthetic Covalent and Non-Covalent 2D Materials, *Angew. Chem*., Int. Ed. 54, 13876 (2015).

12. C. H. Hendon, A. J. Rieth, M. D. Korzy_nski, and M. Dinc_a, Grand Challenges and Future Opportunities for Metal–Organic Frameworks, *ACS Cent*. Sci. 3, 554 (2017).

13. Shams, S. S., Zhang, R. & Zhu, J. Graphene synthesis: A Review. *Materials Science- Poland* **33**, 566–578 (2015).

14. Zhen, Z. & Zhu, H. Structure and Properties of Graphene. in *Graphene* 1–12 (Elsevier, 2018). doi:10.1016/b978-0-12-812651-6.00001-x

15. Papageorgiou, D. G., Kinloch, I. A. & Young, R. J. Mechanical properties of graphene and graphene-based nanocomposites. *Progress in Materials Science* **90**, 75–127 (2017).

16. Pang, S., Hernandez, Y., Feng, X. & Müllen, K. Graphene as transparent electrode material for organic electronics. *Adv. Mater.* **23**, 2779–2795 (2011).

17. Reddy, D., Register, L. F., Carpenter, G. D. & Banerjee, S. K. Graphene field-effect transistors. *J. Phys. D. Appl. Phys.* **44**, 313001 (2011).

18. Xu, C. *et al.* Graphene-based electrodes for electrochemical energy storage. *Energy and Environmental Science* **6**, 1388–1414 (2013).

19. Shao, Y. *et al.* Graphene based electrochemical sensors and biosensors: A review. *Electroanalysis* **22**, 1027–1036 (2010).

20. Jiang, Y., Biswas, P. & Fortner, J. D. A review of recent developments in graphene-enabled membranes for water treatment. *Environ. Sci. Water Res. Technol.* **2**, 915–922 (2016)..

21. Guinea, F., Katsnelson, M. I. & Geim, A. K. Energy gaps and a zero-field quantum hall effect in graphene by strain engineering. *Nat. Phys.* **6**, 30–33 (2010).

22. Cheng, S. H. *et al.* Reversible fluorination of graphene: Evidence of a two-dimensional wide bandgap semiconductor. *Phys. Rev. B - Condens. Matter Mater. Phys.* **81**, (2010).

23. Hicks, J. *et al.* A wide-bandgap metal-semiconductor-metal nanostructure made entirely from graphene. *Nat. Phys.* **9**, 49–54 (2013).

24. S. L. Cai, W. G. Zhang, R. N. Zuckermann, Z. T. Li, X. Zhao, and Y. Liu, The Organic Flatland—Recent Advances in Synthetic 2D Organic Layers, *Adv.Mater*. 27, 5762 (2015).

25. J. W. Colson and W. R. Dichtel, Rationally synthesized two-dimensional polymers *Nat. Chem*. 5, 453 (2013).

26. Yaghi, O. M., & Li, H. (1995). Hydrothermal Synthesis of a Metal-Organic Framework Containing Large Rectangular Channels. *Journal of the American Chemical Society*, 117(41), 10401–10402 (2017).

27. Tranchemontagne, D. J., Hunt, J. R., & Yaghi, O. M. (2008). Room temperature synthesis of metal-organic frameworks: MOF-5, MOF-74, MOF-177, MOF-199, and IRMOF-0. Tetrahedron, 64(36), 8553–8557.

28. Li, H., Eddaoudi, M., O'Keeffe, M., & Yaghi, O. M. (1999). Design and synthesis of an exceptionally stable and highly porous metal-organic framework. *Nature*, 402(6759), 276–279.

29. Chui, S. S. (1999). A Chemically Functionalizable Nanoporous Material [Cu3(TMA)2(H2O)3]n. *Science*, 283(5405), 1148–1150.

30. Furukawa, H. et al. Ultrahigh porosity in metal-organic frameworks. *Science*329, 424-428 (2010).

31. Zhao, M. T. et al. Ultrathin 2D metal-organic framework nanosheets. *Adv. Mater*. 27, 7372-7378 (2015).

32. Qin, J. S. et al. Ultrastable polymolybdate-based metal-organic frameworks a highly active electrocatalysts for hydrogen generation from water. *J. Am. Chem.Soc*. 137, 7196-7177 (2015).

33. Duan, X., Wang, C., Pan, A., Yu, R. & Duan, X. Two-dimensional transition metal dichalcogenides as atomically thin semiconductors: Opportunities and challenges. *Chem. Soc. Rev*. **44**, 8859–8876 (2015).

34. Van Der Zande, A. M. *et al.* Grains and grain boundaries in highly crystalline monolayer molybdenum disulphide. *Nat. Mater*. **12**, 554–561 (2013).

35. Shi, Y. *et al*. Na-assisted fast growth of large single-crystal MoS2 on sapphire. *Nanotechnology* **30**, (2019).

36. Rodenas, T., Luz, I., Prieto, G., Seoane, B., Miro, H., Corma, A., … Gascon, J. (2015). Metal-organic framework nanosheets in polymer composite materials for gas separation. *Nature Materials*, 14(1), 48–55.

37. Li, J. R., Ma, Y., McCarthy, M. C., Sculley, J., Yu, J., Jeong, H. K., … Zhou, H. C. (2011). Carbon dioxide capture-related gas adsorption and separation in metal-organic frameworks. *Coordination Chemistry Reviews*, 255(15–16), 1791–1823.

38. Dong, R., Pfeffermann, M., Liang, H., Zheng, Z., Zhu, X., Zhang, J., & Feng, X. (2015). Large-Area, Free-Standing, Two-Dimensional Supramolecular Polymer Single-Layer Sheets for Highly Efficient Electrocatalytic Hydrogen Evolution. *Angewandte Chemie - International Edition*, 54(41), 12058–12063.

39. Zhao, M., Wang, Y., Ma, Q., Huang, Y., Zhang, X., Ping, J., … Zhang, H. (2015). Ultrathin 2D Metal-Organic Framework Nanosheets. *Advanced Materials*, 27(45), 7372–7378.

40. Li, H., Eddaoudi, M., O'Keeffe, M., & Yaghi, O. M. (1999). Design and synthesis of an exceptionally stable and highly porous metal-organic framework. *Nature*, 402(6759), 276–279.

41. Li, H., Eddaoudi, M., Groy, T. L., & Yaghi, O. M. (1998). Establishing Microporosity in Open Metal−Organic Frameworks: Gas Sorption Isotherms for Zn(BDC) (BDC = 1,4-Benzenedicarboxylate). *Journal of the American Chemical Society*, 120(33), 8571–8572.

42. Chae, H. K., Siberio-Pérez, D. Y., Kim, J., Go, Y., Eddaoudi, M., Matzger, A. J., … Yaghi, O. M. (2004). A route to high surface area, porosity and inclusion of large molecules in crystals. *Nature*, 427(6974), 523–527.

43. Ferey, G. (2005). A Chromium Terephthalate-Based Solid with Unusually Large Pore Volumes and Surface Area. *Science*, 309(5743), 2040–2042.

44. Farha, O. K., Eryazici, I., Jeong, N. C., Hauser, B. G., Wilmer, C. E., Sarjeant, A. a, … Hupp, J. T. (2012). Metal-organic framework materials with ultrahigh surface areas: is the sky the limit? *Journal of the American Chemical Society*, 134(36), 15016–21.

45. Sholl, D. S., & Lively, R. P. (2016). Seven chemical separations to change the world. *Nature*, 532(7600), 435–437.

46. Jana, A. K. (2010). Heat integrated distillation operation. *Applied Energy*, 87(5), 1477–1494.

47. Kaye, S. S., Dailly, A., Yaghi, O. M., & Long, J. R. (2007). Impact of Preparation and Handling on the Hydrogen Storage Properties of Zn4O(1,4-benzenedicarboxylate)3 (MOF-5). *Journal of the American Chemical Society*, 129(46), 14176–14177.

48. Furukawa, H., Miller, M. A., & Yaghi, O. M. (2007). Independent verification of the saturation hydrogen uptake in MOF-177 and establishment of a benchmark for hydrogen adsorption in metal–organic frameworks. *Journal of Materials Chemistry*, 17(30), 3197–3204.

49. Latroche, M., Surblé, S., Serre, C., Mellot-Draznieks, C., Llewellyn, P. L., Lee, J.-H., … Férey, G. (2006). Hydrogen Storage in the Giant-Pore Metal–Organic Frameworks MIL-100 and MIL-101. *Angewandte Chemie International Edition*, 45(48), 8227–8231.

50. Farha, O. K., Özgür Yazaydın, A., Eryazici, I., Malliakas, C. D., Hauser, B. G., Kanatzidis, M. G., … Hupp, J. T. De novo synthesis of a metal–organic framework material featuring ultrahigh surface area and gas storage capacities. *Nature Chemistry*, 2(11), 944–948(2010).

51. Suh, M. P., Park, H. J., Prasad, T. K., & Lim, D.-W. Hydrogen Storage in Metal–Organic Frameworks. *Chemical Reviews*, 112(2), 782–835(2012).

52. Lin, Y. Metal organic framework membranes for separation applications. *Current Opinion in Chemical Engineering*, 8, 21–28(2015).

53. Feng, C., Khulbe, K. C., Matsuura, T., Farnood, R., & Ismail, A. F. *Recent Progress in Zeolite / Zeotype Membranes*, 1, 49–72.(2015)

54. Keskin, S., & Sholl, D. S. Screening metal-organic framework materials for membrane-based methane/carbon dioxide separations. *Journal of Physical Chemistry C*, 111(38), 14055–14059(2007).

55. Liu, Y., Ng, Z., Khan, E. A., Jeong, H.-K., Ching, C., & Lai, Z. (2009). Synthesis of continuous MOF-5 membranes on porous α-alumina substrates. *Microporous and Mesoporous Materials*, 118(1–3), 296–301

56. Huang, A., Chen, Y., Wang, N., Hu, Z., Jiang, J., & Caro, J. (2012). A highly permeable and selective zeolitic imidazolate framework ZIF-95 membrane for H2/CO2 separation. *Chemical Communications*, 48(89), 10981.

57. Matthews, H. D., Gillett, N. P., Stott, P. a, & Zickfeld, K. (2009). The proportionality of global warming to cumulative carbon emissions. *Nature*, 459(7248), 829–32.

58. Figueroa, J. D., Fout, T., Plasynski, S., McIlvried, H., & Srivastava, R. D. (2008). Advances in CO2 capture technology-The U.S. Department of Energy's Carbon Sequestration Program. *International Journal of Greenhouse Gas Control*, 2(1), 9–20

59. Lee, S., & Park, S. (2015). A review on solid adsorbents for carbon dioxide capture. *Journal of Industrial and Engineering Chemistry*, 23, 1–11.

60. Mu, B., & Walton, K. S. (2011). Adsorption equilibrium of methane and carbon dioxide on porous metal-organic framework Zn-BTB. Adsorption-Journal of the International Adsorption Society, 17(5), 777–782.

61. Wang, T., Ge, K., Chen, K., Hou, C., & Fang, M. (2016). Theoretical studies on CO2 capture behavior of quaternary ammonium-based polymeric ionic liquids. *Phys. Chem. Chem. Phys.*, 18(18), 13084–13091.

62. Wang, T., Lackner, K. S., & Wright, A. (2011). Moisture Swing Sorbent for Carbon Dioxide Capture from Ambient Air. Environmental Science & Technology, 45(15), 6670–6675.

63. Wang, T., Liu, J., Lackner, K. S., Shi, X., Fang, M., & Luo, Z. (2016). Characterization of kinetic limitations to atmospheric CO2 capture by solid sorbent. Greenhouse Gases: *Science and Technology*, 6(1), 138–149.

64. D'Alessandro, D. M., Smit, B., & Long, J. R. (2010a). Carbon dioxide capture: Prospects for new materials. Angewandte Chemie - International Edition, 49(35), 6058–6082.

65. Vaidhyanathan, R., Iremonger, S. S., Dawson, K. W., & Shimizu, G. K. H. (2009). An amine-functionalized metal organic framework for preferential CO2 adsorption at low pressures. *Chemical Communications*, (35), 5230.

66. An, J., Geib, S. J., & Rosi, N. L. (2010). High and Selective CO2 Uptake in a Cobalt Adeninate Metal−Organic Framework Exhibiting Pyrimidine- and Amino-Decorated Pores. *Journal of the American Chemical Society*, 132(1), 38–39

67. Bao, Z., Yu, L., Ren, Q., Lu, X., & Deng, S. (2011). Adsorption of CO2 and CH4 on a magnesium-based metal organic framework. *Journal of Colloid and Interface Science*, 353(2), 549–556.

68. Zhai, Q. G., Bu, X., Mao, C., Zhao, X., & Feng, P. (2016). Systematic and Dramatic Tuning on Gas Sorption Performance in Heterometallic Metal-Organic Frameworks. *Journal of the American Chemical Society*, 138(8), 2524–2527.

69. He, H., Song, Y., Zhang, C., Sun, F., Yuan, R., Bian, Z., … Zhu, G. (2015). A highly robust metal–organic framework based on an aromatic 12-carboxyl ligand with highly selective adsorption of CO2 over CH4. *Chemical Communications*, 51(46), 9463–9466.

70. Yaghi, O. M., & Li, H. (1995). Hydrothermal Synthesis of a Metal-Organic Framework Containing Large Rectangular Channels. J*ournal of the American Chemical Society*, 117(41), 10401–10402.

71. M. Zhao, Q. Lu, Q. Ma, and H. Zhang, Two-Dimensional Metal–Organic Framework Nanosheets, *Small Methods* 1, 1600030 (2017).

72. M. Zhao, Y. Huang, Y. Peng, Z. Huang, Q. Ma, and H. Zhang, Two-dimensional metal–organic framework nanosheets: synthesis and applications, *Chem. Soc.Rev*. 47, 6267 (2018).

73. L. Cao, T. Wang, and C. Wang, Chin. Synthetic Strategies for Constructing Two-Dimensional Metal-Organic Layers (MOLs): A Tutorial Review, *J. Chem*. 36, 754 (2018).

74. Y., Biswas, P. & Fortner, J. D. A review of recent developments in graphene-enabled membranes for water treatment. *Environ. Sci. Water Res. Technol.* **2**, 915–922 (2016).

75. Jiang, Y., Biswas, P. & Fortner, J. D. A review of recent developments in graphene-enabled membranes for water treatment. *Environ. Sci. Water Res. Technol.* **2**, 915–922 (2016).

76. Guinea, F., Katsnelson, M. I. & Geim, A. K. Energy gaps and a zero-field quantum hall effect in graphene by strain engineering. *Nat. Phys.* **6**, 30–33 (2010).

77. Duan, X., Wang, C., Pan, A., Yu, R. & Duan, X. Two-dimensional transition metal dichalcogenides as atomically thin semiconductors: Opportunities and challenges. *Chem. Soc. Rev.* **44**, 8859–8876 (2015).

78. Podzorov, V., Gershenson, M. E., Kloc, C., Zeis, R. & Bucher, E. High-mobility field-effect transistors based on transition metal dichalcogenides. *Appl. Phys. Lett.* **84**, 3301–3303 (2004)

79. Wang, J., Verzhbitskiy, I. & Eda, G. Electroluminescent Devices Based on 2D Semiconducting Transition Metal Dichalcogenides. *Advanced Materials* **30**, (2018).

80. Li, B. L. *et al.* Low-Dimensional Transition Metal Dichalcogenide Nanostructures Based Sensors. *Adv. Funct. Mater.* **26**, 7034–7056 (2016).

81. Ruppert, C., Aslan, O. B. & Heinz, T. F. Optical properties and band gap of single- and few-layer MoTe2 crystals. *Nano Lett.* **14**, 6231–6236 (2014).

82. Manzeli, S., Ovchinnikov, D., Pasquier, D., Yazyev, O. V. & Kis, A. 2D transition metal dichalcogenides. *Nat. Rev. Mater.* **2**, 17033 (2017).

83. Cheng, Y. C., Zhu, Z. Y., Tahir, M. & Schwingenschlögl, U. Spin-orbit-induced spin splittings in polar transition metal dichalcogenide monolayers. *EPL* **102**, (2013).

84. Cui, C., Xue, F., Li, L. J. & Hu, W. J. Erratum to: Two-dimensional materials with piezoelectric and ferroelectric functionalities (npj 2D Materials and Applications, (2018), 2, 1, (18), 10.1038/s41699-018-0063-5). *npj 2D Mater. Appl.* **2**, (2018).

85. Tan, X., Smith, S. C. & Dai, Y. A Janus MoSSe monolayer : a superior and. 1099–1106 (2019). doi:10.1039/c8ta08407f

86. Zhang, J. *et al.* Janus Monolayer Transition-Metal Dichalcogenides. *ACS Nano* **11**, 8192–8198 (2017).

87. Ma, X., Yong, X., Jian, C. & Zhang, J. Transition Metal-Functionalized Janus MoSSe Monolayer: A Magnetic and Efficient Single-Atom Photocatalyst for Water-Splitting Applications. *J. Phys. Chem. C* **123**, 18347–18354 (2019).

88. Wagner, R., 309, M. ~, Wagner, R., Raman, A. & Moon, R. *0th International Conference on Wood & Biofiber Plastic Composites ~ Transverse Elasticity of Cellulose Nanocrystals Via atomic Force microscopy*.

89. Raman Scattering in Fluorescence Emission Spectra | Common Errors. Available at: https://www.edinst.com/us/blog/raman-scattering-blog/. (Accessed: 30th October 2019)

90. Princeton Instruments General Raman. Available at: https://www.princeton instruments.com/applications/raman-gen. (Accessed: 30th October 2019)

91. Choi, W. *et al.* Recent development of two-dimensional transition metal dichalcogenides and their applications. *Materials Today* **20**, 116–130 (2017).

92. Merlo, A., Mokkapati, V. R. S. S., Pandit, S. & Mijakovic, I. Boron nitride nanomaterials: Biocompatibility and bio-applications. *Biomater. Sci.* **6**, 2298–2311 (2018).

93. Chae, H. K., Siberio-Pérez, D. Y., Kim, J., Go, Y., Eddaoudi, M., Matzger, A. J., … Yaghi, O. M. (2004). A route to high surface area, porosity and inclusion of large molecules in crystals. *Nature*, 427(6974), 523–527..

94. Kang, Z., Fan, L., & Sun, D. (2017). Recent advances and challenges of metal–organic framework membranes for gas separation. *J. Mater. Chem.* A, 5(21), 10073–10091.

95. Sengupta, A., Datta, S., Su, C., Herng, T. S., Ding, J., Vittal, J. J., & Loh, K. P. (2016). Tunable Electrical Conductivity and Magnetic Property of the Two Dimensional Metal Organic Framework [Cu(TPyP)Cu2(O2CCH3)4]. ACS Applied Materials and Interfaces, 8(25), 16154–16159.

96. Makiura, R., Motoyama, S., Umemura, Y., Yamanaka, H., Sakata, O., & Kitagawa, H. (2010). Surface nano-architecture of a metal-organic framework. *Nature Materials*, 9(7), 565–571.

97. Rodenas, T., Luz, I., Prieto, G., Seoane, B., Miro, H., Corma, A., … Gascon, J. (2015). Metal-organic framework nanosheets in polymer composite materials for gas separation. *Nature Materials*, 14(1), 48–55.

98. Amo-Ochoa, P., Welte, L., González-Prieto, R., Sanz Miguel, P. J., Gómez-García, C. J., Mateo-Martí, E., … Zamora, F. (2010). Single layers of a multifunctional laminar Cu(i,ii) coordination polymer. *Chemical Communications*, 46(19), 3262–3264.

99. Li, J. R., Ma, Y., McCarthy, M. C., Sculley, J., Yu, J., Jeong, H. K., … Zhou, H. C. (2011). Carbon dioxide capture-related gas adsorption and separation in metal-organic frameworks. *Coordination Chemistry Reviews*, 255(15–16), 1791–1823..

100. Yuxia Shen, Bohan Shan, Bin Mu, S. Tongay(2020). Achieving Morphological Control over Lamellar Manganese Metal-Organic Framework through Modulated Bi-Phase Growth. *Commun doi:* 10.1002/anie.202002705 (2020)

101. Yuxia Shen, Bohan Shan,…., Bin Mu, S. Tongay Ultimate Control over Hydrogen Bond Formation and Reaction Rates for Scalable Synthesis of Highly Crystallin vdW MOF Nanosheets with Large Aspect Ratio. *Adv. Mater*. 2018, 30, 1802497

102. Jingrun Ran, Jiangtao Qu, Hongping Zhang,……, Rongkun Zheng, and Shi-Zhang Qiao. 2D Metal Organic Framework Nanosheet: A UniversalPlatform Promoting Highly Efficient Visible-Light-Induced Hydrogen Production. *Adv. Energy Mater*. 2019, 1803402

103. Suh, M. P., Park, H. J., Prasad, T. K., & Lim, D.-W. (2012). Hydrogen Storage in Metal–Organic Frameworks. *Chemical Review*s, 112(2), 782–835.

104. D'Alessandro, D. M., Smit, B., & Long, J. R. (2010a). Carbon dioxide capture: Prospects for new materials. *Angewandte Chemie* - International Edition, 49(35), 6058–6082. http://doi.

105. Jingrun Ran,……., 2D Metal Organic Framework Nanosheet: A Universal Platform Promoting Highly Efficient Visible-Light-Induced Hydrogen Productionpaper. Adv. Energy Mater. 2019, 1803402

106. S. Tongay, J. Hwang, D. B. Tanner, H. K. Pal, D. Maslov, A. F. Hebard, Supermetallic conductivity in bromine-intercalated graphite. *Phys. Rev*. B 2010, 81, 115428;

107. X. Meng, A. Pant, H. Cai, J. Kang, H. Sahin, B. Chen, K. Wu, S. Yang, A.Suslu, F. M. Peeters, S. Tongay, Engineering excitonic dynamics and environmental stability of post-transition metal chalcogenides by pyridine functionalization technique. *Nanoscale* 2015, 7, 17109 – 17115

108. M. S. Whittingham, R. R. Chianelli, Layered compounds and intercalation chemistry: An example of chemistry and diffusion in solids. J. *Chem. Educ.* 1980, 57, 569

109. Y. He, B. Chen, Metal–Organic Frameworks: Frameworks Containing Open Sites. *Encyclopedia of Inorganic and Bioinorganic Chemistry*, 1-23 (2014).

110. Patricia Silva,Sergio M.F,J PC Tome, Multifunctional metal–organic frameworks: from academia to industrial applications. *Chem. Soc. Rev*., 2015, 44, 6774--6803

111 I.-F. Chen, C.F. Lu, and W.F. Su, Highly Conductive 2D Metal-Organic Framework Thin Film Fabricated by Liquid-Liquid Interfacial Reaction Using One-Pot-Synthesized Benzenehexathiol. *Langmuir* 34, 15754 (2018).